



Michigan Technological University
Create the Future Digital Commons @ Michigan Tech

Dissertations, Master's Theses and Master's
Reports - Open

Dissertations, Master's Theses and Master's
Reports

2014

EXPERIMENTAL SETUP AND CONTROLLER DESIGN FOR AN HCCI ENGINE

Deepak Kothari
Michigan Technological University

Follow this and additional works at: <https://digitalcommons.mtu.edu/etds>


 Part of the [Automotive Engineering Commons](#)

Copyright 2014 Deepak Kothari

Recommended Citation

Kothari, Deepak, "EXPERIMENTAL SETUP AND CONTROLLER DESIGN FOR AN HCCI ENGINE", Master's Thesis, Michigan Technological University, 2014.
<https://digitalcommons.mtu.edu/etds/963>

Follow this and additional works at: <https://digitalcommons.mtu.edu/etds>

 Part of the [Automotive Engineering Commons](#)

EXPERIMENTAL SETUP AND CONTROLLER DESIGN FOR AN HCCI ENGINE

By

Deepak Kothari

A THESIS

Submitted in partial fulfillment of the requirements for the degree of

MASTER OF SCIENCE

In Mechanical Engineering

MICHIGAN TECHNOLOGICAL UNIVERSITY

2014

© 2014 Deepak Kothari

This thesis has been approved in partial fulfillment of the requirements for the Degree of
MASTER OF SCIENCE in Mechanical Engineering.

Department of Mechanical Engineering - Engineering Mechanics

Thesis Advisor: *Dr. Mahdi Shahbakhti*

Committee Member: *Dr. Scott A Miers*

Committee Member: *Dr. Mohsen Azizi*

Department Chair: *Dr. William W. Predebon*

To My Family, Mentors, Friends and Michigan Tech

“If you think you can you will and if you think you can’t you won’t ”
.....by Henry Ford

Contents

List of Figures	xi
List of Tables	xv
List of Abbreviations	xvii
Acknowledgments	xxiii
Abstract	xxv
1 Introduction	1
1.1 Background	1
1.2 Principles and Working of HCCI Engines	4
1.3 History of HCCI Engines	5
1.4 Actuation Methods for Controlling Combustion in HCCI Engines	6
1.5 Emissions in HCCI Engines	8
1.6 Problem Identification and Research Scope	9
1.7 Thesis Organization	11
2 Engine Instrumentation and Controller Setup	13
2.1 Base Engine Description	13
2.2 Engine Test Setup	15
2.3 Data Acquisition and Control Units	17
2.4 Engine Sensors and Actuators	19
2.4.1 Lambda Sensor (Wide Band O ₂ Sensor)	21

2.4.2	Electronic Throttle Control (ETC) Valve	22
2.4.3	Exhaust Gas Recirculation (EGR) Valve	23
2.4.4	Crank/Cam Position Sensors for Engine Synchronization	25
2.4.5	Port Fuel Injectors	26
2.5	Summary	27
3	HCCI control oriented model	29
3.1	Control Oriented Model	29
3.2	HCCI Engine Cycle Model	30
3.2.1	Induction Stroke	30
3.2.2	Compression Stroke	32
3.2.3	Combustion Period	32
3.2.3.1	Start of Combustion (SOC) and CA50 Prediction	32
3.2.3.2	End of Combustion (EOC)	35
3.2.4	Expansion Stroke	37
3.2.5	Exhaust Stroke	37
3.3	Exhaust Gas Temperature Model	38
3.4	Indicated Mean Effective Pressure (IMEP) Model	39
3.5	Thermocouple Lag	41
3.6	Transient Validation of COM	41
3.7	Model Summary	42
4	HCCI Controller Design	43
4.1	Introduction of Controllers	43
4.1.1	Single-Output vs. Multi-Output Controllers	44
4.1.2	Empirical Controllers vs. Model-Based Controllers	45
4.2	Controller Test Bed	47
4.2.1	Single-Input Single-Output (SISO) Controllers	47
4.2.1.1	Discrete PID Controller for CA50	47

4.2.1.2	Discrete PID Controller for T_{exh}	49
4.2.1.3	DSSMC for CA50	50
4.2.1.4	DSSMC for T_{exh}	54
4.2.2	Two-Input Two-Output Controller	58
4.2.2.1	Discrete PID Controllers for CA50 and T_{exh}	58
4.2.2.2	DSSMCs for CA50 and T_{exh}	60
4.2.3	Comparisons of Two-Input Two-Output Controllers	62
4.3	Three-Input Three-Output Controller	64
4.4	Controllers' Summary	68
5	Conclusion and Future Work	71
5.1	Summary	71
5.2	Suggestions for Future Work	72
	References	75
	A Acronyms for different LTC Engines	83
	B MSc. Publication	85
	C Thesis Files Summary	87

List of Figures

1.1	Primary Energy Flow in USA for 2011 (Quadrillion BTU) (Data source: [1])	2
1.2	Major HCCI Benefit (Green Circles) and Drawbacks (Dashed Red Circles)	3
1.3	Combustion in HCCI Engine Versus Diesel Engine and SI Engine . . .	5
1.4	One Complete Combustion Cycle in HCCI Engine	8
1.5	Thesis Structure	11
2.1	Schematic of the 2.0-L Ecotec LHU Engine	14
2.2	Valve Timing of 2.0-L Ecotec LHU Engine	15
2.3	Schematic of the HCCI Engine Experimental Setup	16
2.4	Actual Engine Experimental Setup	16
2.5	High Level Structure of HCCI Engine ECU	19
2.6	dSPACE Simulink Screen Shot	20
2.7	Position of Bosch Lambda Sensors Installed : (1) Before the Intake Manifold, and (2) Exhaust Pipe of the Engine	21
2.8	Step Response of the ETC Valve	23
2.9	Side and Bottom Views of the EGR Valve	24
2.10	Step Response of the EGR Valve	24
2.11	Verifying Firing TDC Using In-cylinder Pressure Voltage Signal and Crank Angle Using DS1637 RapidPro Module. (Engine Motoring Speed = 1000 rpm)	26
2.12	PFI Injector and Crank Position Sensor Signal	27

2.13 Engine Sensors and Controller Units. Dashed lines Show Planned Future Work.	28
2.14 Engine Actuators and Controller Units. Dashed lines Show Planned Future Work.	28
3.1 Comparison Between CA50 Prediction from MKIM and CA50 Correlation, RMSE Stands for Root Mean Square Error	34
3.2 Steady State Validation for CA50 Correlation	35
3.3 Schematic of the Control Volume for T_{exh} Model	39
3.4 Steady State Validation for T_{exh} Physical Model	40
3.5 Steady State Validation for IMEP Model	40
3.6 Validation of the COM for Transient Engine Operation. (a _x): Model and Experimental Data Comparison and (b _x): Inputs to the HCCI engine. P_{man} , T_{man} , N and % EGR are 110 kPa, 91 °C, 815 rpm and 0 % Respectively	42
4.1 Control Background of the HCCI Engines in Literature	45
4.2 Structure of CA50 PID Controller	48
4.3 Tracking Performance of CA50 PID Controller. (a): Plant Output and (b): Control Input	48
4.4 Structure of T_{exh} PID Controller	49
4.5 Tracking Performance of T_{exh} PID Controller. (a): Plant Output and (b): Control Input	49
4.6 Structure of CA50 DSSMC	54
4.7 Tracking Performance of CA50 DSSMC. (a): Plant Output and (b): Control Input	55
4.8 Structure of T_{exh} DSSMC	55
4.9 Tracking Performance of T_{exh} DSSMC. (a): Plant Output and (b): Control Input	57
4.10 Structure of the MIMO PID Controller to Control CA50 and T_{exh}	59

4.11 Single Tracking Performance of CA50 and T_{exh} by PID Controllers. (a_x): Plant Outputs and (b_x): Control Inputs	59
4.12 Simultaneous Tracking Performance of CA50 and T_{exh} by PID Controllers. (a_x): Plant Outputs and (b_x): Control Inputs	60
4.13 Structure of the MIMO DSSMCs to Control CA50 and T_{exh} . W_1 and W_2 are the Disturbance Simulated using the Plant Model	61
4.14 Single Tracking Performance of CA50 and T_{exh} by DSSMCs. (a_x): Plant outputs and (b_x): Control inputs	62
4.15 Simultaneous Tracking Performance of CA50 and T_{exh} by DSSMCs. (a_x): Plant Outputs and (b_x): Control Inputs	63
4.16 Controller A - Structure of MIMO Empirical Controller to Control CA50, T_{exh} and IMEP	65
4.17 Controller B - Structure of Combined MIMO Model-Based / Empirical Controller to Control CA50, T_{exh} and IMEP. W_1 and W_2 are the Disturbance Simulated using the Plant Model	66
4.18 Comparing Single Tracking Performance for Three-Input Three-Output, Type A (Fig.4.16) and Type B (Fig.4.17) Controllers. (a_x): Plant Outputs and (b_x): Control Inputs	67
4.19 Comparing Simultaneous Tracking Performance for Three-Input Three-Output, Type A (Fig.4.16) and Type B (Fig.4.17) Controllers. (a_x): Plant Outputs and (b_x): Control Inputs	68
4.20 Tracking Error Comparison for Three-Input Three-Output, Type A (Fig.4.16) and Type B (Fig.4.17) Controllers for the Single Tracking Changes, where (a_x) are the Plant Outputs	69
4.21 Tracking Error Comparison for Three-Input Three-Output, Type A (Fig.4.16) and Type B (Fig.4.17) Controllers for the Simultaneous Tracking Changes, where (a_x) are the Plant Outputs	70

List of Tables

1.1	California Air Resources Board (CARB) Emission norms [2]	2
1.2	Milestone Achieved by Researcher in Development of HCCI Engines	7
2.1	2.0-L Ecotec LHU Engine Specification	14
2.2	Sensors in Engine (Internal and External)	17
2.3	Actuators in Engine (Internal and External)	17
2.4	dSPACE RapidPro Modules and their Applications	18
3.1	Ricardo Engine Specification	30
3.2	Range of HCCI Engine Operating Conditions to Carry Out MKIM Simulations	34
3.3	Operating Range of Experimental Data for Steady State Validation	34
3.4	Accuracy of the COM for the Transient Engine Operation in Fig.3.6	41
4.1	Nominal Operating Point Around Which the Nonlinear COM is Linearized	46
4.2	Range of Input Parameters for the HCCI Plant Model	47
4.3	Tracking Performance For Designed SISO Controllers	58
4.4	Tracking and Disturbance Rejection Performance of Two-Input Two-Output Controllers	64
4.5	Tracking and Disturbance Rejection Performance of Three-Input Three-Output Controllers	70
A.1	Acronym of Different LTC Engines	84

C.1	Experimental Data Files (.mat files)	88
C.2	Simulink Models Files (.slx files)	88
C.3	Documents	88
C.4	Matlab Script Files (.m files)	89
C.5	Matlab Figures Files (.fig files)	90
C.6	Vision Drawings/Images Files	91

List of Abbreviation

Φ	Equivalence ratio
ρ	Density [kg/m ³]
aBDC	after Bottom Dead Center
AFR _{st}	Air-Fuel Stoichiometric Ratio
aTDC	after Top Dead Center
BDC	Bottom Dead Center
bTDC	before Top Dead Center
C _v	Average gas specific heat capacity [KJ/kg-K]
CA50	Crank Angle at 50% mass fuel burn [CAD]
CAD	Crank Angle Degree
CAN	Controller Area Network
CARB	California Air Resources Board
CI	Compression Ignition
CO	Carbon Monoxide

CO ₂	Carbon Dioxide
CoC	Completeness of Combustion
COM	Control Oriented Model
DI	Direct Injector
DSSMC	Discrete Sub-optimal Sliding Mode Controller
ECU	Engine Control Unit
EGR	Exhaust Gas Recirculation
EOC	End Of Combustion
ETC	Electronic Throttle Control
EU	European Standards
EVC	Exhaust Valve Closing
EVO	Exhaust Valve Opening
GTDI	Gasoline Turbocharged Direct Injection
h	Heat transfer coefficient [W/m ² -K]
HC	Hydrocarbon
HCCI	Homogeneous Charge Compression Ignition
HCHO	Formaldehyde
I _p	Pump current [A]
IC	Internal Combustion

IMEP	Indicated Mean Effective Pressure [bar]
IVC	Intake Valve Closing
IVO	Intake Valve Opening
K_c	Specific heat capacity ratio at compression
K_d	Derivative gain
K_e	Specific heat capacity ratio at expansion
K_i	Integral gain
K_p	Proportional gain
LEV	Low Emission Vehicle
LHV	lower Heating Value [kJ/kg]
LSD	Low Side Driver
LTC	Low Temperature Combustion
m_{fuel}	Mass of fuel
m_t	Total mixture mass
MABX	MicroAutoBox
MAF	Mass Air Flow
MAP	Manifold Air Pressure
MIMO	Multi Input Multi Output
MKIM	Modified Knock Integral Model

N	Engine speed [rpm]
N ₂	Nitrogen
NMOG	Non Methane Organic Gas
NO _x	Nitrogen Oxide
NVO	Negative Valve Overlap
O ₂	Oxygen
ON	Octane Number
P _{exh}	Pressure at exhaust manifold
P _{ivc}	Pressure at intake valve closing
P _{man}	Intake manifold pressure
P _{soc}	Pressure at start of combustion
PFI	Port Fuel Injector
PI	Proportional Integral
PID	Proportional Integral Derivative
PM	Particulate Matter
PPS	Pintle Position Sensor
PS	RapidPro power unit
Q	Heat energy
Q _{corr}	Correction factor

R	Gas constant [kJ/kg-K]
RCP	Rapid Control Prototyping
RGF	Residual Gas Fraction
RMSE	Root Mean Square Error
SC	RapidPro control unit
SI	Spark Ignition
SISO	Single Input Single Output
SOC	Start Of Combustion
SOI	Start Of Injection
STD	Standard Deviation
SULEV	Super Ultra-Low Emission Vehicle
$T_{ambient}$	Ambient Temperature
T_{evc}	Temperature at exhaust valve closing
T_{exh}	Exhaust gas temperature
T_{ivc}	Temperature at intake valve closing
T_{man}	Temperature at intake manifold
T_{mix}	Modified temperature at intake valve closing
T_{rg}	Temperature of residual gases
T_{soc}	Temperature at start of combustion

TDC	Top Dead Center
TLA	Thermodynamics Loss Angle
TPS	Throttle Position Sensor
U	Internal energy
U_A	Pump current Volatge [V]
ULEV	Ultra Low Emission Vehicle
V_{dis}	Displacement Volume
V_{ivc}	Volume at intake valve closing
V_{soc}	Volume at start of combustion
VVT	Variable Valve Timing
W	Work Done
W_k	Disturbance
ZEV	Zero Emission Vehicle
ZIF	Zero Insertion Force

Acknowledgments

I would like to thank all my family members for giving me unconditional support for each and every step of my life.

I would like to express my sincere gratitude to my adviser Dr.Mahdi Shahbakhti for granting me an opportunity to work within EML group at MTU. I immensely appreciate his continuous support and motivation for my master's research. I am very thankful for his effort in teaching me true meaning of "Quality Work". I would also like to thank Dr.Scott A Miers and Dr.Mohsen Azizi for participating member for my thesis defense committee.

I would like to thank my group for helping me in completing my tasks. I would like to express my immense gratitude to Mehran for helping me understand the clear task for my research. I would also like to appreciate Hrishikesh, Dennis, Vishal, Anup, Kaveh, Shivaram, Ninad, Harshith, Ajinkiy, Sunit, Ravi, Jaydev, Fouad and Abhishek for helping me in developing experimental test cell. I truly appreciate your hard work, it would have been never possible without your efforts.

I would like to thank Paul, Sean, Martin and Steven for their advice, knowledge and patience for helping me understand all related task for my projects. I wanted to thanks Meysam and Mohammad for helping me learn latex. I wanted to thank Yash, Pranjali, Harriet, Mehran and Anup for helping me editing my draft.

Last but not least, I would like to thanks all my friends. You all are special and have a very important role in my simple life. Thank you for giving me continuous inspiration, for all your best knowledge a 'meaningless name' has tremendous motivation.

Abstract

Homogeneous charged compression ignition (HCCI) is a promising combustion mode for internal combustion (IC) engines. HCCI engines have very low NO_x and soot emission and low fuel consumption compared to traditional engines. The aim of this thesis is divided into two main parts: (1) engine instrumentation with a step towards converting a gasoline turbocharged direct injection (GTDI) engine to an HCCI engine; and (2) developing controller for adjusting the crank angle at 50% mass fuel burn (CA50), exhaust gas temperature T_{exh} , and indicated mean effective pressure (IMEP) of a single cylinder Ricardo HCCI engine.

The base GTDI engine is modified by adding an air heater, inter-cooler, and exhaust gas recirculation (EGR) in the intake and exhaust loops. dSPACE control units are programmed for adding monitoring sensors and implementing actuators in the engine. Control logics for actuating electronic throttle control (ETC) valve, EGR valve, and port fuel injector (PFI) are developed using the rapid control prototyping (RCP) feature of dSPACE. A control logic for crank/cam synchronization to determine engine crank angle with respect to firing top dead center (TDC) is implemented and validated using in-cylinder pressure sensor data.

A control oriented model (COM) is developed for estimating engine parameters including CA50, T_{exh} , and IMEP for a single cylinder Ricardo engine. The COM is validated using experimental data for steady state and transient engine operating conditions. A novel three-input three-output controller is developed and tested on a detailed physical HCCI engine plant model. Two type of controller design approaches are used for designing HCCI controllers: (1) empirical, and (2) model-based. A discrete sub-optimal sliding mode controller (DSSMC) is designed as a model-based controller to control CA50 and T_{exh} , and a PI controller is designed to control IMEP. The results show that the designed controllers can successfully track the reference trajectories and can reject the external disturbances

within the given operating region.

Chapter 1

Introduction

1.1 Background

IC engines have three important features associated with them: (1) fuel consumption, (2) efficiency, and (3) emissions. Today, engineers and scientists are working continuously to optimize these three features. Fuel blending, intake air pressure boosting, EGR, fuel additive, design improvement, direct injection (DI), and variable valve timing (VVT) are among some of the techniques for making IC engines more fuel efficient and environmentally friendly.

According to data collected by the World Bank, the energy usage and carbon dioxide (CO₂) emissions throughout the world have increased by double from 1975 to 2010 [3]- [4]. Fig.1.1 shows that in the USA, almost 28% of energy is used by the automobile sector, among which 93% comes from fossil fuel base sources. These numbers indicate two of the most crucial areas which are drastically impacted on a large scale: (1) limitation of fuel supply in the future, and (2) adverse effects on the environment due to increased quantities

of greenhouse gases. Because of increasing detrimental effects caused by automobile pollutants, governments are forcing automobile manufacturers to improve their technology by implementing stringent emissions norms. Table 1.1 shows the norms for California Air Resources Board (CARB) emission standards for controlling emissions.

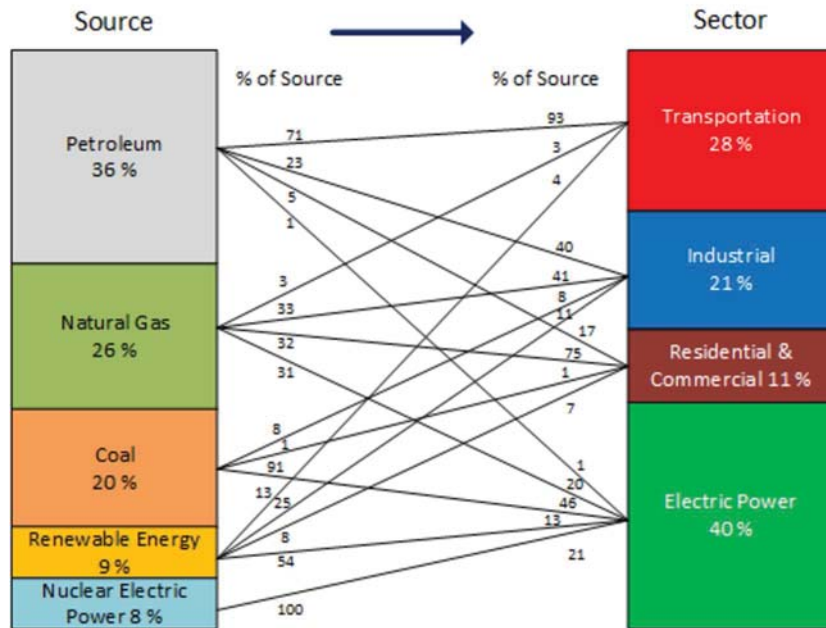


Figure 1.1: Primary Energy Flow in USA for 2011 (Quadrillion BTU) (Data source: [1])

Table 1.1
California Air Resources Board (CARB) Emission norms [2]

California Emission Standard	Year		CO (g/mi)	HCHO (g/mi)	NOMG + NO _x (g/mi)	PM (g/mi)
Passenger Car	2015-2025	LEV	4.2	4	0.16	0.01
		ULEV	1.7	4	0.05	0.01
		SULEV	1	4	0.02	0.01

For automobile manufacturers, the ultimate emissions goal is to produce zero emission vehicles (ZEV) with optimized performance and minimum cost. Although fuel cell and

electric vehicles are some of the promising options for achieving ZEV, but they do not offer the required energy density in relation to cost effectiveness [5].

Due to the absence of efficient batteries, it is very clear that first steps should be towards improving IC engine technology. Over the last 15 years, a significant amount of research has been conducted on HCCI engines, which are a type of low temperature combustion (LTC) engine. These engines can be defined as a hybrid of spark ignition (SI) and compression ignition (CI) engines and are a good alternative to traditional technology. Some of the benefits and challenges faced by HCCI engines are highlighted in Fig.1.2.

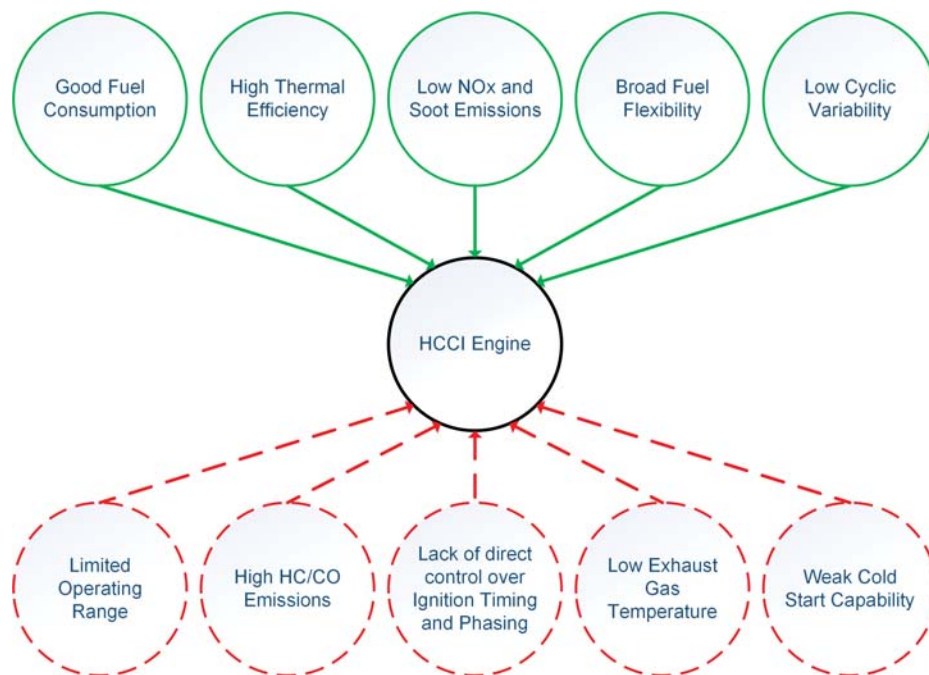


Figure 1.2: Major HCCI Benefit (Green Circles) and Drawbacks (Dashed Red Circles)

Interest in HCCI engines has grown because of increases in fuel prices with simultaneous decreases in fuel quantity, and stringent emissions standards. These engines have the potential to improve the internal combustion engine's efficiency and fuel consumption, and to reduce nitrogen oxide (NO_x) and particulate matter (PM) emissions with negligible soot [6]. Realization of HCCI into production faces the following vital challenges:

1. limitations on operating load and speed
2. lack of control over combustion phasing
3. higher hydrocarbon (HC) and carbon monoxide (CO) emissions
4. weak cold start capability
5. low exhaust gas temperature to heat up catalytic converter

1.2 Principles and Working of HCCI Engines

In an HCCI engine, the formation of the air fuel mixture is similar to that of an SI engine (homogeneous mixture) and initiation of combustion is similar to a CI engine (auto ignition at the end of the compression stroke). Therefore it is reasonable to define an HCCI engine as a hybrid of SI and CI engines. For combustion to happen in an HCCI engine, it is important that during the compression stroke the mean temperature of the charge mixture reaches auto ignition temperature or the engine will misfire. This temperature criteria is achieved either by constraining hot residual gas or by heating intake air. In an HCCI engine, auto ignition happens throughout the combustion chamber, as shown in Fig.1.3. That is, combustion happens at multiple points throughout the combustion chamber, resulting in simultaneous heat release events without any flame propagation. This process was verified through spectroscopic and imaging investigations by the Lund Institute of Technology [7]- [8].

Multiple parallel auto ignition points in an HCCI engine lead to rapid heat release rates for a shorter combustion duration when compared to SI and CI engines. There are two main controls which have to be satisfied in order to attain proper HCCI combustion: (1) control of combustion near the vicinity of top dead center (TDC), and (2) control of the heat release rate during high load and high speed operating conditions. Failure may lead to improper combustion and knocking effects [9]. To avoid failure during high load and high

speed conditions, an HCCI engine should run either in lean conditions or incorporate high amounts of dilute residual gases.

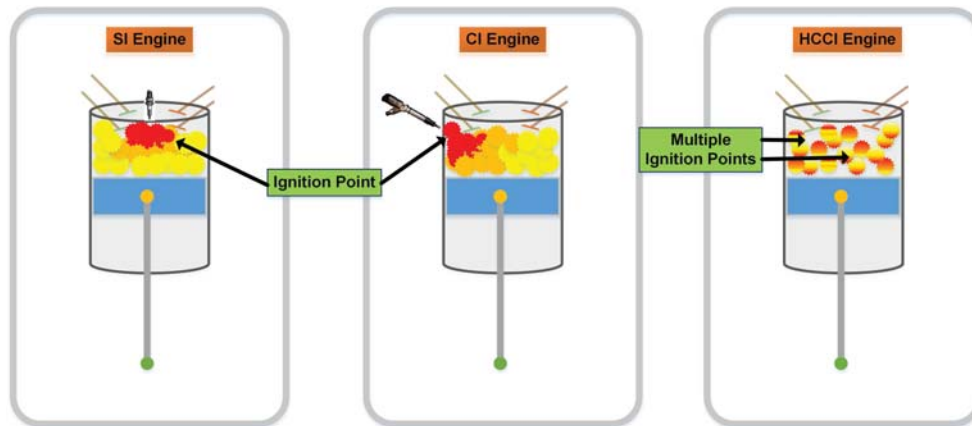


Figure 1.3: Combustion in HCCI Engine Versus Diesel Engine and SI Engine

The phenomenon of heat release characteristics in an HCCI engine differs from an SI or CI engine. In SI engines, heat released is confined by a reaction zone, which is a thin layer between burned and unburned mixtures inside a combustion chamber. In CI engines, the majority of the heat release is achieved by diffusive burning of air fuel mixture. In an HCCI engine, all mixtures instantaneously take part in the heat release process during combustion. Therefore, total heat released in an HCCI engine is the sum of heat released by all the individual reactions in the combustion chamber [6].

1.3 History of HCCI Engines

During their development, both SI and CI engines have experienced the similar type of combustion process as studied in recent HCCI engines. For example, the SI engine can experience the ‘after-run or run on’ phenomenon when the carburetor was used for mixing air and fuel [6]. This often happened after switching the engine OFF. Hundred years

ago the hot bulb oil engine [10], a type of CI engine, used a separate heated chamber for vaporizing fuel before insertion into the main combustion chamber. This leads to a homogenous charge mixture which assists in auto ignition's combustion similarly to the HCCI engine. Table 1.2 shows some of the milestones achieved by researchers in the past in the field of HCCI engines.

1.4 Actuation Methods for Controlling Combustion in HCCI Engines

The working of an HCCI engine consists of six steps in one complete cycle as shown Fig.1.4: (1) compression, (2) auto ignition, (3) expansion, (4) exhaust, (5) residual

Table 1.2
Milestone Achieved by Researcher in Development of HCCI Engines

Sr/no	Work
1	1930s, Nikolai Semenov [6], generate root of HCCI combustion concept by doing first chemical kinetics controlled combustion study for diesel engine
2	1970s, Gussak, Karpov and Tikhonov, from Academy of Sciences of the USSR [11], developed first controlled combustion engine, using partial burned mixture from separate chamber
3	1979, Onishi and Noguchi [12]- [13], HCCI research in 2 stroke engine
4	1983, Najt and Foster, Univ of Wisconsin Madison [14], HCCI research in 4 stroke engine
5	1989, Thring [15], tested effects of air fuel ratio and EGR on engine performance. Also he introduces the name "Homogeneous Charged Compression Ignition (HCCI) Engine"
6	1992, V. Stockinher, H. Schapertons and U. Kuhkmann [16], first time explorer the operating region (limited speed and load) of 4 stroke gasoline engine in auto ignition mode by increasing compression ratio and heating intake air
7	1990, Lund Institute of Technology [17], developed 12 liter-6 cylinder largest gasoline engine running in auto ignition mode by using mixture of two fuels (heptane and iso-octane), increasing compression ratio, heating intake air and booting intake air by turbo charger
8	2001, Lotus Engineering Ltd. [18], first to use of exhaust valve closing (EVC) and negative valve overlap (NVO) for HCCI engine combustion, operating in limited speed and load range by using fully flexible variable valve actuation
9	2003, AVL list GmbH [19], Explorer nature of residual gas fraction and exhaust rebreathing in order to achieve HCCI combustion in available production engines, stating best method for fuel consumption and most promising feature for HCCI to come closer to production line
10	2007, GM [20] demonstrated HCCI engine working, in powertrain of Opel Vectra and Saturn Aura with maximum speed of 60 MPH
11	2014, BOSCH, et al. [21] developed mode switching engine between SI and HCCI engine, named as SACI-HCCI engine

recompression and, (6) induction. An HCCI engine lacks a direct actuation step for initiating combustion, like a spark plug in an SI engine or a fuel injector in a diesel engine. Thus, there is a need for an actuation strategy to initiate combustion within the combustion cycle. Some control actuation strategies which are commonly used to support combustion

events in HCCI engines are as follows.

1. intake air heating [16]
2. variable compression ratio [22]
3. variable valve timing [23]
4. external EGR [15]
5. internal EGR by negative valve overlap (NVO) [18]
6. internal EGR by exhaust rebreathing [19]
7. multiple fuels [17]
8. multiple in-cylinder fuel injections [24]

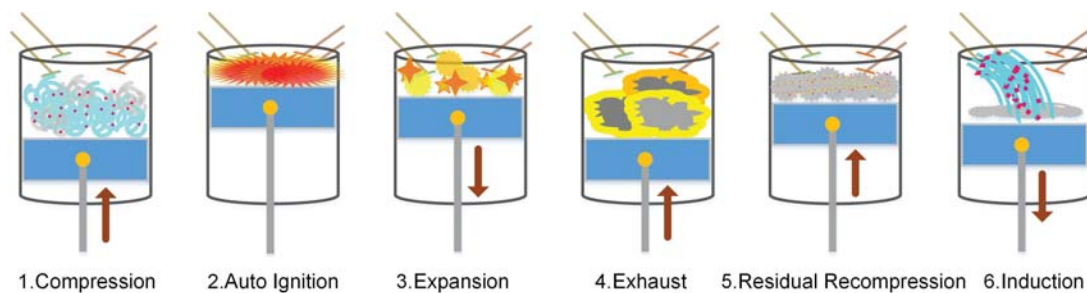


Figure 1.4: One Complete Combustion Cycle in HCCI Engine

1.5 Emissions in HCCI Engines

In the development of advanced methods in IC engines, emissions are one of the most important factors which have to be studied. There are two important factors which dictate the nature of emissions for any IC engines, (1) in-cylinder peak combustion temperature, and (2) in-cylinder charge composition [9]. The following are some of the commonly known emissions and their effects on HCCI engines:

1. NO_x Emission - Some of the important mechanisms for formation of NO_x in IC engines are: thermal or zeldovich mechanism, Fenimore or promote mechanism, N_2O -intermediate mechanism, NNH mechanism [25]. The minimum activation temperature required for breaking the N_2 bond is approximately 1800K. In the case of an HCCI engine, the peak temperature of combustion remains below 1800K due to the lean and dilute mixture. This inhibits breaking the N_2 triple bonds and therefore avoids NO_x formation. SI and CI engines temperature can go as high as 2500K, which exponentially increases formation of NO_x during exhaust. Hence NO_x emission in an HCCI engine is significantly smaller compared to their counterpart SI and CI engines.
2. Soot - The main factor for soot formation in an IC engine is because of the rich mixture region which lacks a complete breakdown of hydrocarbon due to insufficient availability of oxygen at the time of combustion [9]. But in the case of HCCI engines, the charge inducted in the combustion chamber is leaner and well mixed (homogeneously mixture), which inhibits the formation of pockets of the hydrocarbon chains, thus removing the cause for soot formation.
3. HC/CO emission - In-cylinder peak temperature is an important factor in deciding the HC/CO emission from an IC engine. Lower in-cylinder temperatures result in increased emissions. The low peak in-cylinder temperature of an HCCI engine creates a major challenge to limit these emissions.

1.6 Problem Identification and Research Scope

According to a report given by Department of Energy - Energy, Efficiency and Renewable energy (EERE) office to U.S congress on HCCI technology [26], “Reduction of HC and CO emissions from IC engines are easier than reduction of NO_x and soot emissions”. HCCI engines already have a capability of getting rid of NO_x and soot emissions

and thus potentially removing NO_x and soot after treatment systems. Despite all the given advantages of an HCCI engine (shown in Fig.1.2), HCCI engines fall short in controlling high amounts of CO and HC emissions compared to their counterpart SI and CI engines [27].

In [28], an experimental investigation on a single cylinder modified Ricardo HCCI engine was performed. 340 steady state operating points along with varying transient conditions were studied. It was observed that for the majority of operating conditions, the exhaust gas temperature measures were below 300°C . Low exhaust gas temperatures lead to low catalytic converter efficiency (reduce oxidation efficiency [29]).

With the help of a catalytic converter, almost 90-95 % of CO and HC emissions can be removed, but only if the catalytic converter is working at its required operating temperature [30]. For most of the catalytic converters present today, the light off temperature is in the range of $250 - 300^\circ\text{C}$ [31]- [32]. Light off temperature is defined as the temperature at which a catalytic converter system 50% effective. For an HCCI engine, because of its low exhaust gas temperature, it is difficult for a catalytic converter to work at its optimal condition. There are methods available which can help reduce the catalytic light off temperature but will end up increasing the cost of the system [33].

Thus, there is a need for a strategy which can adjust engine parameters like combustion timing at 50% mass fuel burn (CA50), exhaust gas temperature (T_{exh}) and indicated mean effective pressure (IMEP) in order to enhance the working limits of HCCI engine. The goal of this thesis is to develop an efficient controller, which can simultaneously adjust these three output parameters by adjusting octane number (ON), intake manifold pressure (P_{man}) and mass flow rate of fuel (\dot{m}_{fuel}), respectively. In addition, the thesis includes initial steps for developing engine controller and instrumentation for the HCCI experimental test cell at Michigan Technological University.

1.7 Thesis Organization

This thesis is organized into five different chapters briefly described in Fig.1.5. Chapter 1 gives a brief overview of history, fundamentals, advantages, and challenges faced by an HCCI engine. Chapter 2 gives an overview of experimental engine setup. In Chapter 3, a mathematical control oriented model (COM) is developed to simulate the working of a single cylinder HCCI engine. This model includes an HCCI engine cycle model, an exhaust gas temperature model and an IMEP model. Chapter 4 includes the design of empirical based and model-based HCCI engine controllers to adjust three main engine parameters including CA_{50} , T_{exh} , and IMEP. Finally, Chapter 5 summarizes all major results from the thesis and provides recommendations for future research to expand the results from this thesis.

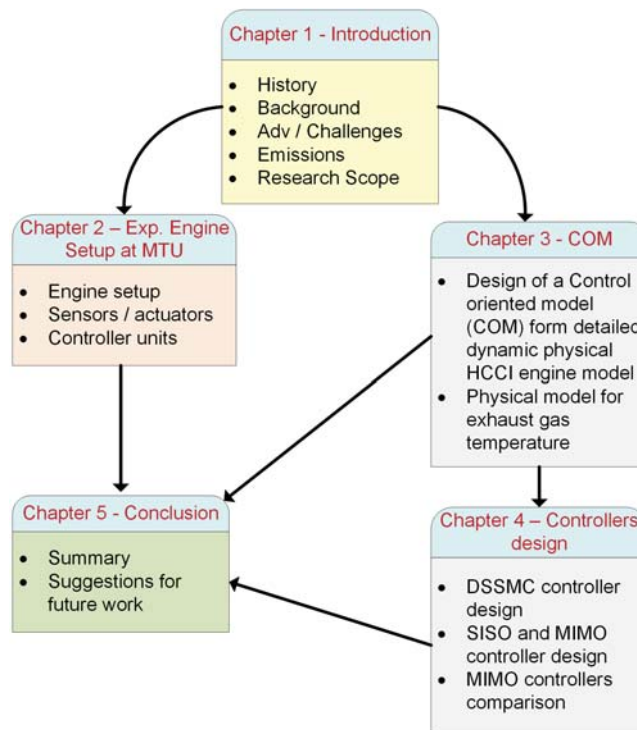


Figure 1.5: Thesis Structure

Chapter 2

Engine Instrumentation and Controller Setup

2.1 Base Engine Description

A GM Ecotec 2.0-liter Gen I LHU engine was selected as a base engine for building an HCCI engine. This chapter gives an overview about an HCCI engine test setup with focus on the sensor instrumental and engine controller setup. The base engine is an in-line four-cylinder GTDI with VVT. Schematic, valve timing, and specification of this engine are shown in Fig.2.1, Fig.2.2, and Table 2.1. This engine was taken from a 2011 Buick Regal (vehicle). Some of the major highlights of this engine are as follows:

1. direct injection: fuel system operating at pressure as high as 2250 psi
2. dual overhead cam shaft with cam phaser
3. hydraulic vane-type phasers for both intake and exhaust cam shafts
4. twin-scroll turbocharger, with boost up to 20 psia
5. capacity of producing 220 horsepower and 353 Nm torque

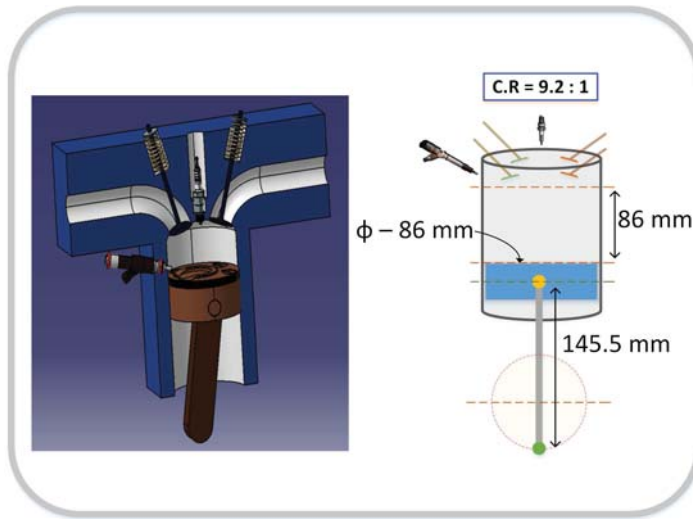


Figure 2.1: Schematic of the 2.0-L Ecotec LHU Engine

Table 2.1
2.0-L Ecotec LHU Engine Specification

Bore	86 mm
Stroke	86 mm
Number of cylinders	4
Compression ratio	9.2 : 1
Connecting rod length	145.5 mm
Displacement volume	1998 cc
Clearance volume	61 cc
Firing order	1-3-4-2
Intake valve opening (park position)	31.25° aTDC
Exhaust valve opening (park position)	39.25° bBDC
Intake valve lift	10.3 mm
Exhaust valve lift	10.3 mm
Intake valve duration	197.5°
Exhaust valve duration	187°
CAM phasing	66°

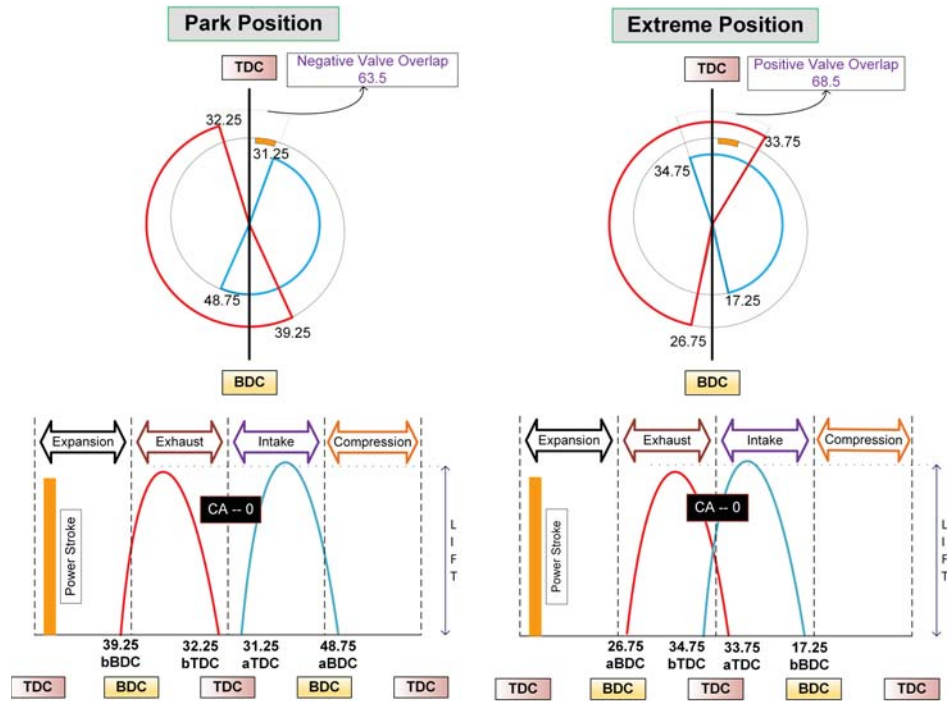


Figure 2.2: Valve Timing of 2.0-L Ecotec LHU Engine

2.2 Engine Test Setup

The LHU Ecotec engine is modified in terms of intake and exhaust loops and additional sets of sensors and actuators are installed on the base engine for monitoring and optimizing engine performance. Fig.2.3 shows an overall engine setup along with a majority of sensors and actuators. Sensors and actuators which were present in the production engine are denoted as internal sensors/actuators in this thesis (e.g. crank position sensor, spark plug, etc.) and sensors/actuators which were installed to add further controllability in the HCCI operation are denoted as external sensors/actuators (e.g. in-cylinder pressure sensors, crank shaft encoder, EGR valve, etc.). Table 2.2 and Table 2.3, list all internal and external sensors and actuators in the engine setup.

A number of thermocouples and pressure transducers are probed inside different loops and

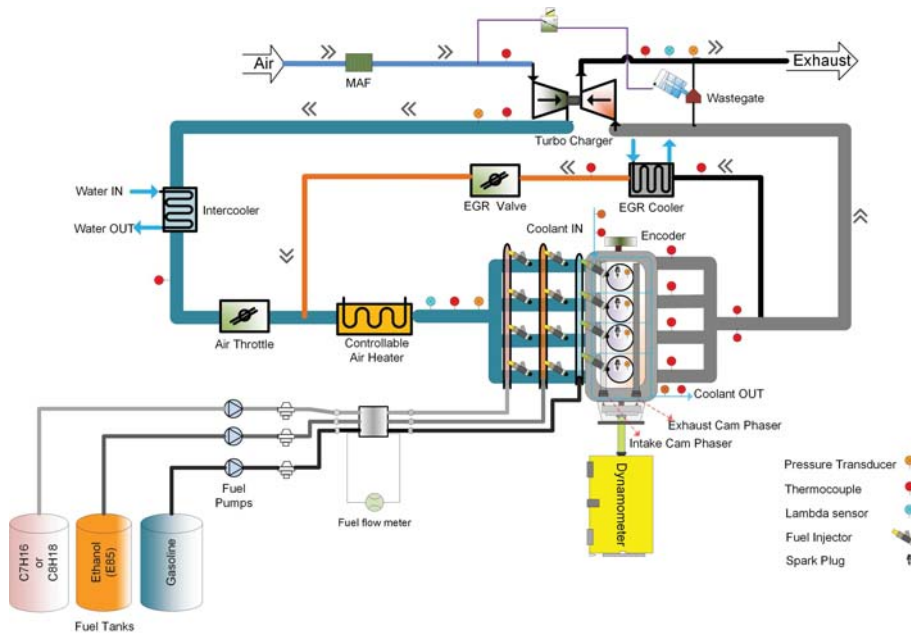


Figure 2.3: Schematic of the HCCI Engine Experimental Setup

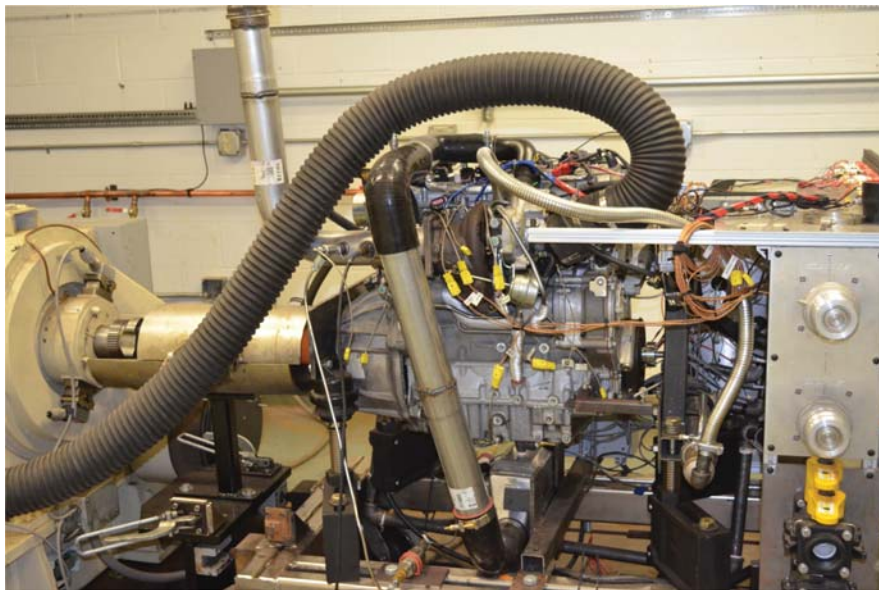


Figure 2.4: Actual Engine Experimental Setup

sections of the setup to help monitor different sections of the engine during HCCI operating conditions. Two wide band lambda sensors are installed in the setup, one near the intake manifold and the other in the exhaust runner to calculate $\%O_2$, EGR amount, and λ value of the exhaust gases. An intercooler is installed in the intake loop for cooling and increasing

density of hot compressed air from the turbocharger. Similarly, one more cooler is added to the EGR loop to control temperature of the recirculated gases. A air heater is added to the intake path, to control intake air temperature. Future steps include adding PFI injectors, supercharger system, and using new designed pistons to increase compression ratio to 12:1. This will help in developing the transition from a base GTDI engine to an HCCI engine.

Table 2.2
Sensors in Engine (Internal and External)

Sensors	
Internal	External
MAP sensor	Themocouples
MAF sensor	In-cylinder pressure transducers
Rail pressure sensor	Pressure transducers
Knock sensor	Lambda sensors
Crank position sensor	Encoder
Cam intake/exhaust position sensors	

Table 2.3
Actuators in Engine (Internal and External)

Actuators	
Internal	External
Electronic thorttle valve	EGR valve
Direct fuel injectors	Port fuel injectors
Spark plugs	
Fuel pump regulators	
Intake/exhaust cam phasers	Air heater
Waste gate valve	

2.3 Data Acquisition and Control Units

Two dSPACE control units are programmed for controlling engine actuators and acquiring data from engine sensors. dSPACE units include: (1) MicroAutoBox (MABX) II; and (2) RapidPro unit. In addition, an Omega air heater controller is used to control intake air

temperature. A THMM mini thermoscan module and NI PXI 4353 is used for temperature data acquisition. Some other modules from NI system are used for testing, i.e. NI PXI 6225 for analog input (e.g. pressure transducer), PXI 6722 for analog output (e.g. water control valve), PXI 6225-SCB0 for digital input/output, and PXI 6143 for frequency (e.g. mass air flow (MAF) sensor).

MABX II (1401/1511/1512) is used in this study because this dSPACE unit provides rapid control prototyping (RCP) capability for engine control unit (ECU) controller design. MABX II includes a set of three compiled boards in which 1401 is a processor board. Some of the features of the DS1401 board include: PPC750 GL Power PC, 900 MHz clock frequency, and real-time clock; 8 MB global RAM memory, 16 MB local RAM, and 16 MB flash memory. MABX II uses DS1511 and DS1512 I/O boards to acquire analog signals (0-5 V), provide signals (0-4.5 V), and control area network (CAN) communication.

RapidPro is a slave unit which gets access via a MABX master unit by CAN communication. The RapidPro includes two main units: (1) RapidPro power unit (PS); and (2) RapidPro control unit (SC). These units are further divided in different modules. All the modules from dSPACE RapidPro unit are listed in Table 2.4. The PS unit is used for controlling some actuators and the SC unit is used for acquiring data from different engine sensors.

Table 2.4
dSPACE RapidPro Modules and their Applications

Rapid Pro module	Application
SC-EGOS 2/1 (DS1634)	Lambda sensor
SC-CCDI 6/1 (DS1637)	Crank and cam position sensor
SC-KNOCK 4/1 (DS1635)	Knock sensor
SC-DO 8/1 (DS1647)	Spark plug
PS-LSD 6/1 (DS1662)	Port fuel injectors, cam phasers and EGR valve
PS-FBD 2/1 (DS1661)	Electronic throttle valve
PS-DINJ 2/1 (DS1664)	Direct injectors

2.4 Engine Sensors and Actuators

A high level control structure for the HCCI engine ECU is shown in Fig.2.5. The dSPACE unit monitors sensors, including throttle position sensor (TPS), EGR valve pintle position sensor (PPS), crank/cam position sensors, thermocouples, and lambda sensors. These sensors are used for making control logic for crank/cam synchronization and controlling actuators including ETC valve, EGR valve, spark plugs, DI, and PFI injectors.

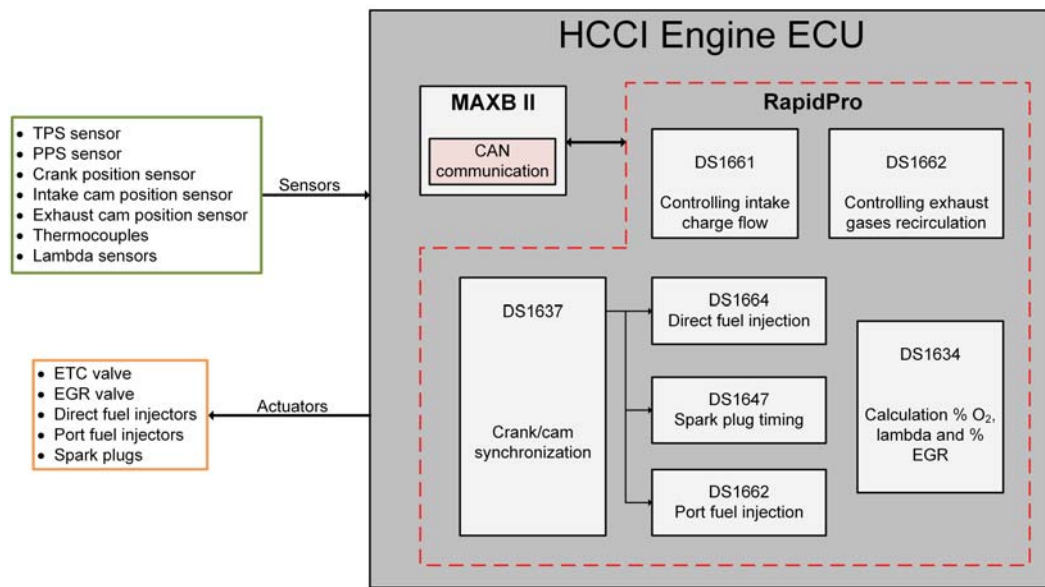


Figure 2.5: High Level Structure of HCCI Engine ECU

Fig.2.6 gives an overall Simulink model (using dSPACE blocksets) for monitoring and actuating some of the sensors and actuators of the engine. Blocksets RCPU_SETUP_BL1 and RCPU_TIMER_SETUP_TPU_BL1 are used for initializing the dSPACE hardware units. CAN_TYPE1_SETUP_M1_C1 is used for defining the CAN network between MAXB and other processors by initializing a .dbc file. THMM_18142_MSGO is a CAN receiver block for the THMM processor for thermocouples' temperature measurements. Blocksets RPCU_CRANK_SETUP_TPU_BL1 and RPCU_CAM_TPU_BL1

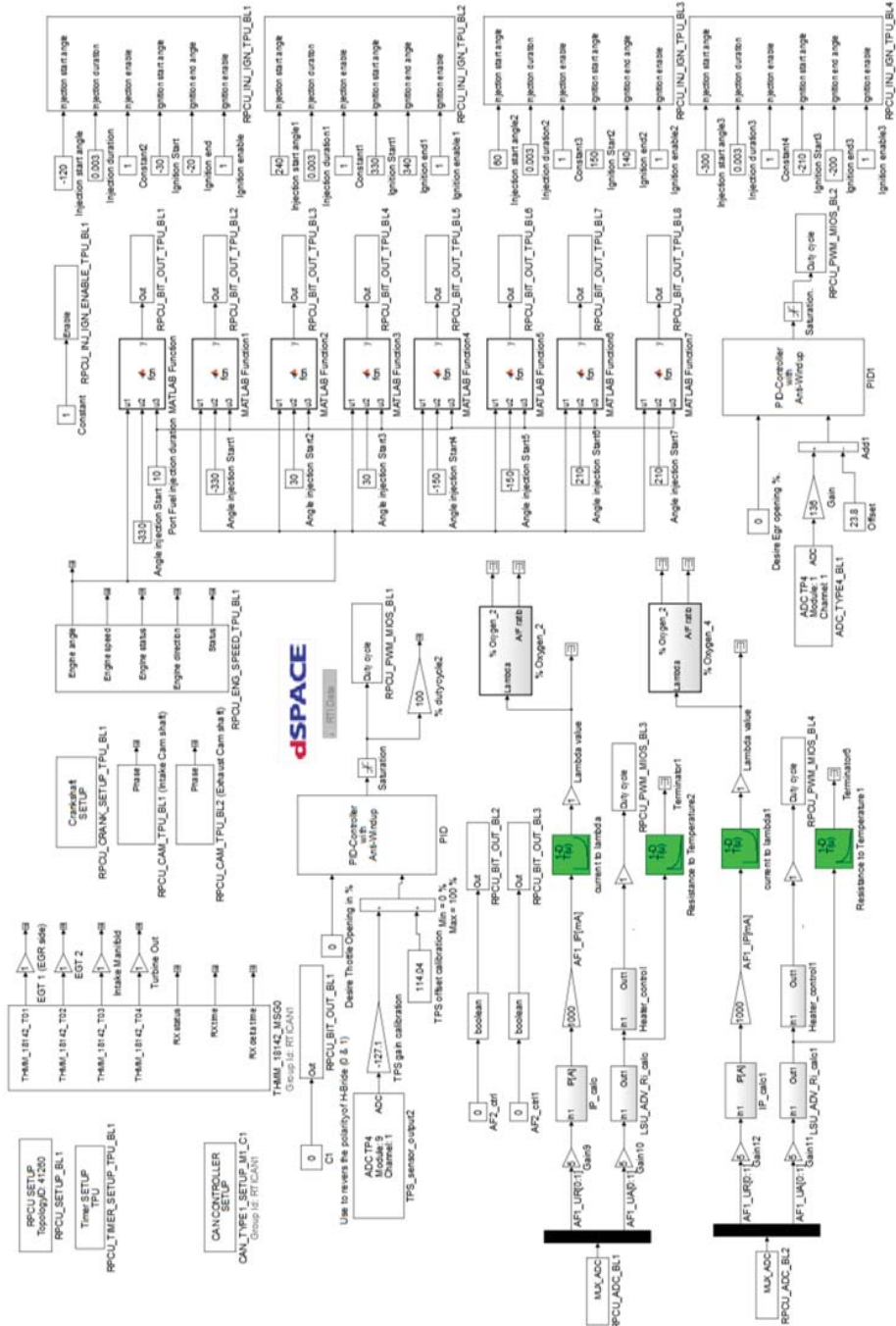


Figure 2.6: dSPACE Simulink Screen Shot

are used for defining crank and cam specification and `RPCU_ENG_SPEED_TPU_BL1` provide engine speed and synchronized engine crank angle. `RPCU_BIT_OUT_TPU_BL1` and `RPCU_PWM_MISO_BL1` are used for regulating duty cycle for controlling actuators

including port fuel injectors, throttle, and EGR valve. Blocksets ADC_TYPE_BL1 and RPCU_ADC_BL1 are used for measuring the analog voltage signals from sensors. Finally, RPCU_INJ_IGN_TPU_BL1 is used for actuating direct fuel injectors and the spark plug of the engine.

Fig.2.6 shows simulink blocks of some sensors and actuators which are monitored and controlled using dSPACE control units:

2.4.1 Lambda Sensor (Wide Band O₂ Sensor)

Two Bosch lambda sensors are installed in the engine setup as shown in the engine schematic Fig.2.3. These sensors are also known as wide band sensors and have capability of measuring λ ranging from 0.65 to infinity. These sensors are used for measuring lambda from exhaust gases and % oxygen in the intake manifold to calculate EGR. Fig.2.7 is an image of the lambda sensors installed in the engine setup.

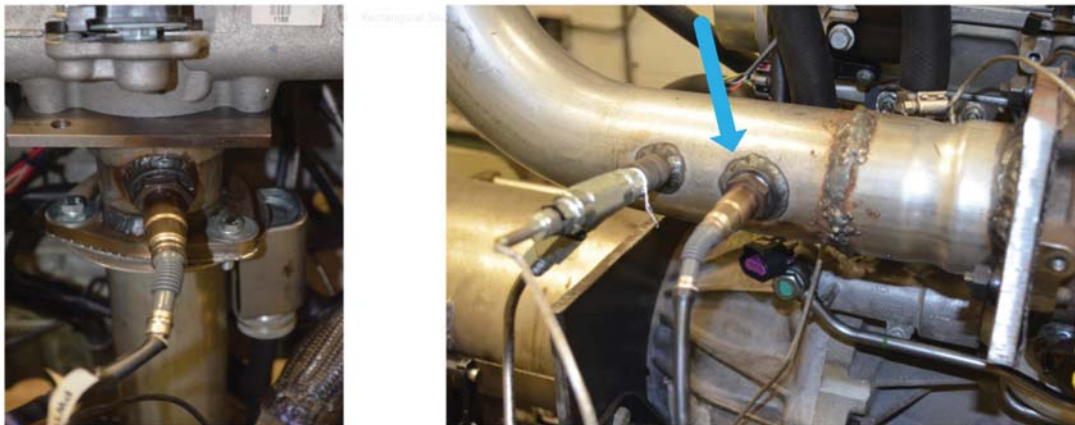


Figure 2.7: Position of Bosch Lambda Sensors Installed : (1) Before the Intake Manifold, and (2) Exhaust Pipe of the Engine

The Bosch LSU 4.9 lambda sensor also has an integral heater attached to it. This heater allows the sensor to warm up automatically till the engine exhaust gas gets warmed up and

further maintains the temperature using an integral controller. DS1662, a low side driver (LSD) module from RapidPro along with constant 12 volt power supply, is used to control the lambda sensor integral heater. The output of the lambda sensor (i.e. pump current voltage) is connected to the DS1634 module of the RapidPro. The measured pump voltage is converted to pump current using Eq.(2.1), and is further converted to lambda and % oxygen using the lookup table from the sensor manual.

$$I_p = \frac{U_A - 1.5}{496} \quad (2.1)$$

where I_p is pump current in [A] and U_A is pump voltage in [V].

2.4.2 Electronic Throttle Control (ETC) Valve

The engine uses an ETC valve to control the intake air flow rate. The original ETC was controlled by production ECU. For an HCCI engine the ETC control strategy differs from production strategy, thus new dSPACE control logic is designed to control the ETC.

There are two important components present in the ETC: (1) TPS (sensor); and (2) servomotor controlled valve (actuator). The TPS is used for providing feedback signals to the ECU based on the valve position. An external source with a 5 volt power supply is required to activate the TPS sensor. The DS1661 module from the RapidPro unit is used to actuate the servomotor inside the valve assembly.

A proportional-integral-derivative (PID) controller is designed which works on a basis of error between the desired set point of throttle position and the actual position given by the calibrated TPS. The tuned gain values for the PID controller are: $K_p = 3$, $K_i = 1$, and $K_d = 0.025$. Fig.2.8 shows controller performance for a step response. The ETC controller performance metrics are: rise time = 0.05 sec, settling time = 0.25 sec, %overshoot =

25.9%, and the steady-state error = 0.5% of the valve opening.

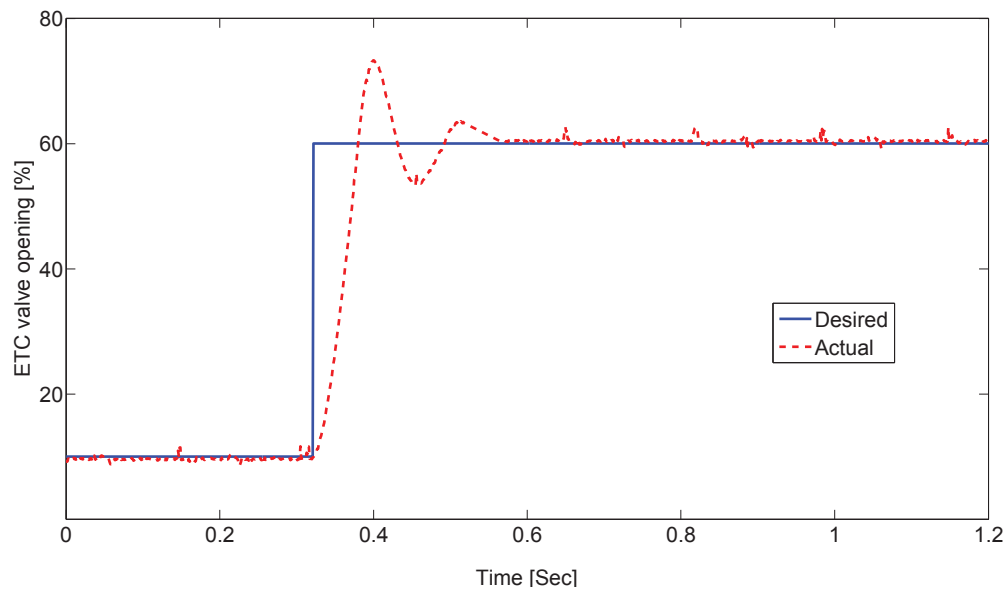


Figure 2.8: Step Response of the ETC Valve

2.4.3 Exhaust Gas Recirculation (EGR) Valve

EGR can be used in HCCI engines to decrease knocking tendency, expand operating region and also increase intake charge temperature for auto-ignition. A custom made loop for an external EGR is developed during the engine setup (Fig.2.3), including an attached EGR cooler and an EGR valve. This loop starts from the exhaust manifold and ends up after the air heater and before the intake manifold. The EGR valve works on the basis of pintle linear movement. Fig.2.9 shows the side view and bottom view image of the EGR valve used.

Similar to TPS in the ETC valve, EGR has a PPS sensor attached to it which provides a feedback signal for controlling the pintle position. A constant 5 volt power supply is required for the sensor to remain activated. The DS1662 module from the RapidPro unit is used as a LSD for a constant 12 volt power supply for the solenoid actuator.

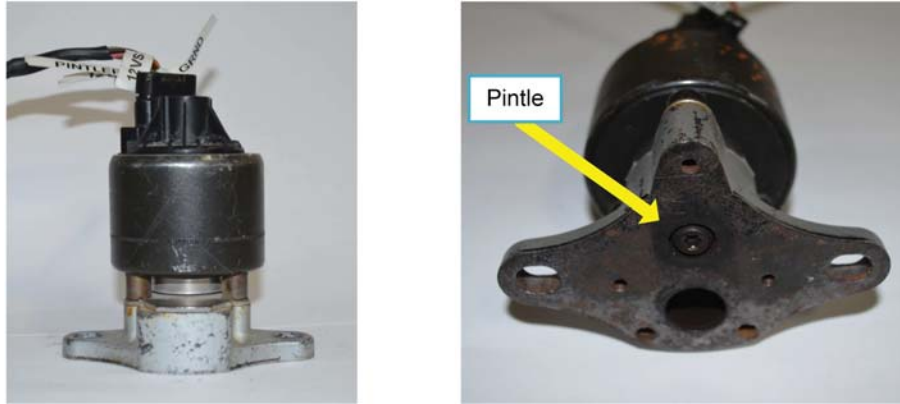


Figure 2.9: Side and Bottom Views of the EGR Valve

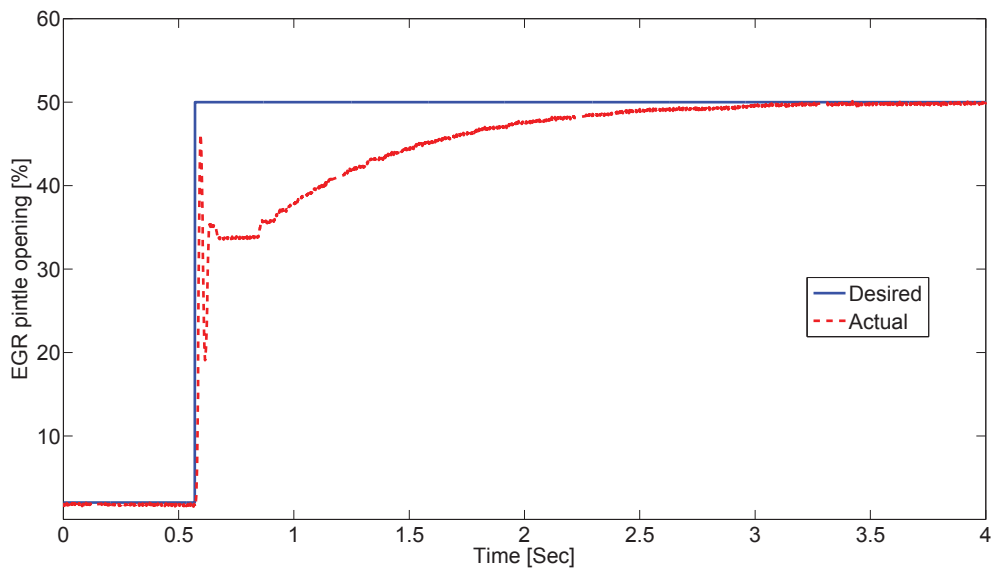


Figure 2.10: Step Response of the EGR Valve

A proportional-integral (PI) controller is developed in order to control the pintle position. The tuned gain values for the PI controller are: $K_p = 0.5$ and $K_i = 0.95$. Fig.2.10 shows the performance of the EGR valve controller. The EGR controller performance metrics are: rise time = 0.01 sec, settling time = 2.05 sec, % overshoot = 0%, and the steady-state error = 0.45% of pintle opening.

2.4.4 Crank/Cam Position Sensors for Engine Synchronization

One main application of crank/cam position sensors is for engine synchronization. It is one of the most crucial tasks for ECU development for actuators like injectors, spark plug, phasers, etc. The synchronize signal helps to determine the crank angle with respect to the firing TDC. For computing crank angle, sensor signals are retrieved from the crank shaft position sensor and intake/exhaust cam shaft position sensors. These are rooted to the DS1637 module of the RapidPro. The crank and cam position sensors are hall effect type and these sensors only require a 5 volt power supply for activation. Along with these position sensors, in-cylinder pressure data is also monitored. The sensors data is combined to find the location of firing TDC of the engine. Some of the specifications of crank and cam position sensors, which are required to complete crank/cam synchronization in the RapidPro (i.e. RPCU engine), are as follows:

1. Crank specification:

Number of crankshaft teeth = 60

Missing teeth per gap = 2

Number of gap = 1

2. Intake cam specification:

Number of camshaft pulses = 4 (2 wide 2 short)

Crank angle is estimated with the rise in pulses of the intake cam wheel with respect to missing teeth from the crank shaft wheel. The estimated values are 204, 384, 444 and 624 crank angle degrees, respectively.

3. Exhaust cam specification:

Number of camshaft pulses = 4 (2 wide 2 short)

Crank angle is estimated with the rise in pulses of the exhaust cam wheel with respect to missing teeth from the crank shaft wheel. The estimated values are 294, 474, 534 and 714 crank angle degrees, respectively.

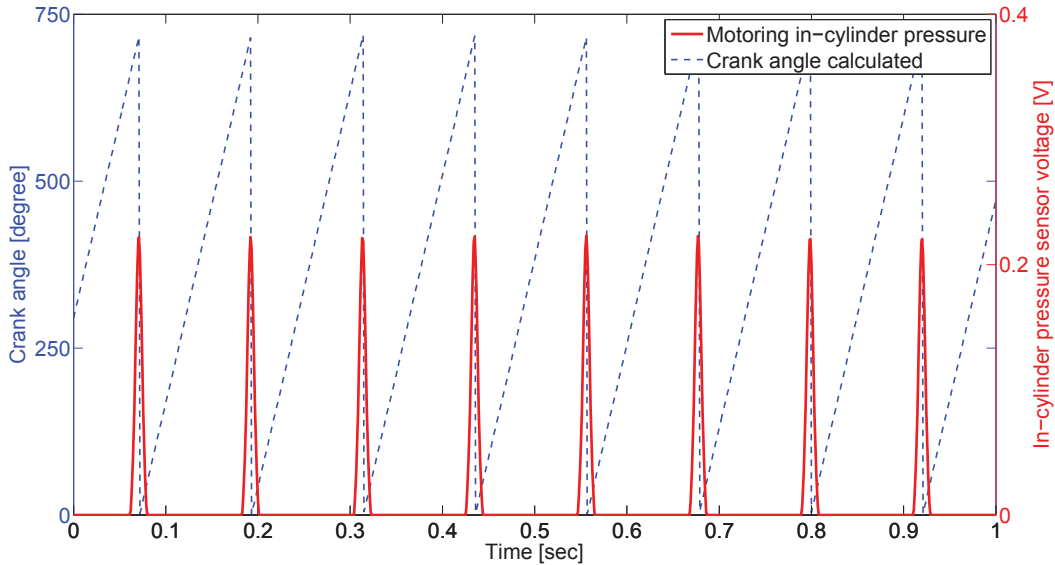


Figure 2.11: Verifying Firing TDC Using In-cylinder Pressure Voltage Signal and Crank Angle Using DS1637 RapidPro Module. (Engine Motoring Speed = 1000 rpm)

Fig.2.11, verifies the calculated crank angle obtained using the DS1637 module of the RapidPro by comparing it with in-cylinder pressure sensor voltage values when the engine is in a motoring condition. It should be noted that the peak value of the in-cylinder pressure sensor is not exactly at the point of firing TDC, instead it is $1^\circ - 2^\circ$ before TDC. This is because of the thermodynamic loss angle (TLA) [34].

2.4.5 Port Fuel Injectors

A set of two port fuel injectors (PFI) per cylinder is planned to be added to the base engine (i.e. 8 port fuel injectors in total as shown in Fig.2.3). This will assist the HCCI engine to operate in combination with fuel flex control logics. Bosch EV-14 PFI fuel injectors

are selected because of their twin spray and cone angle pattern which causes minimal fuel impingement on the intake ports wall and allows better mixing before entering the combustion chamber. A control logic is developed for actuating PFI injectors based on engine angle, start of injection (SOI), and injection duration. The LSD (DS1662) module is used for actuating PFI injectors. Fig.2.12 shows the PFI actuating signal along with the signal from the crank position sensor. It should be noted for testing purposes, SOI and injection duration are set to be 30 bTDC and 20 CAD, respectively.

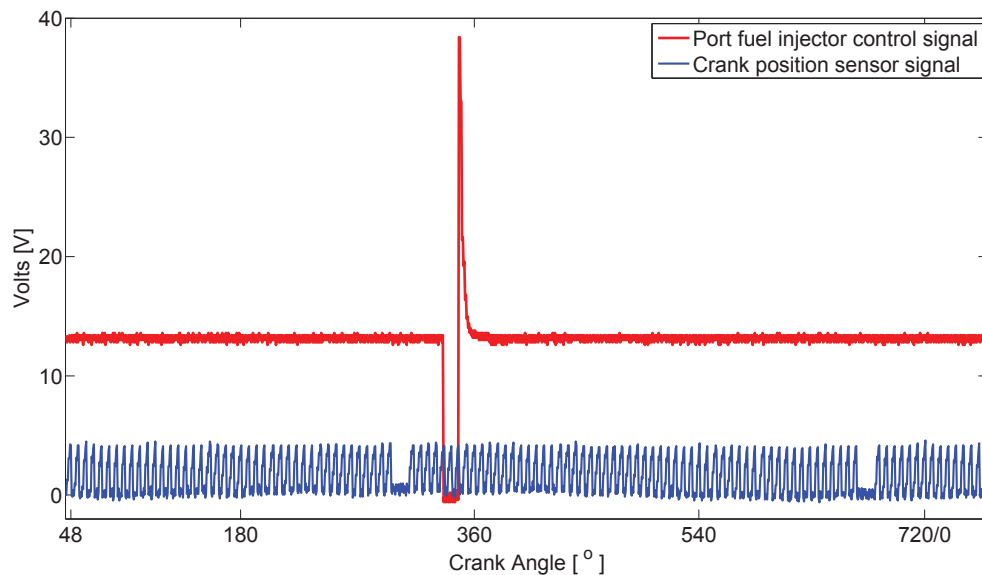


Figure 2.12: PFI Injector and Crank Position Sensor Signal

2.5 Summary

In this chapter an overview of engine instrumentation and controller setup for the HCCI experimental setup was provided. Fig.2.13 and Fig.2.14 give a brief summary of the HCCI engine's sensors and actuators, along with the control units. Here the 'dSPACE' include THMM mini module, MAXB, and RapidPro controllers; and the 'DAQ system' includes NI-PXI modules, Omega controller, variable frequency driver (VFD), and ACAP systems.

Sensors and actuators represented in green and yellow boxes are external and internal sensors/actuators, respectively. It should be noted that all dashed line bordered sensors and actuators are future tasks to be completed.

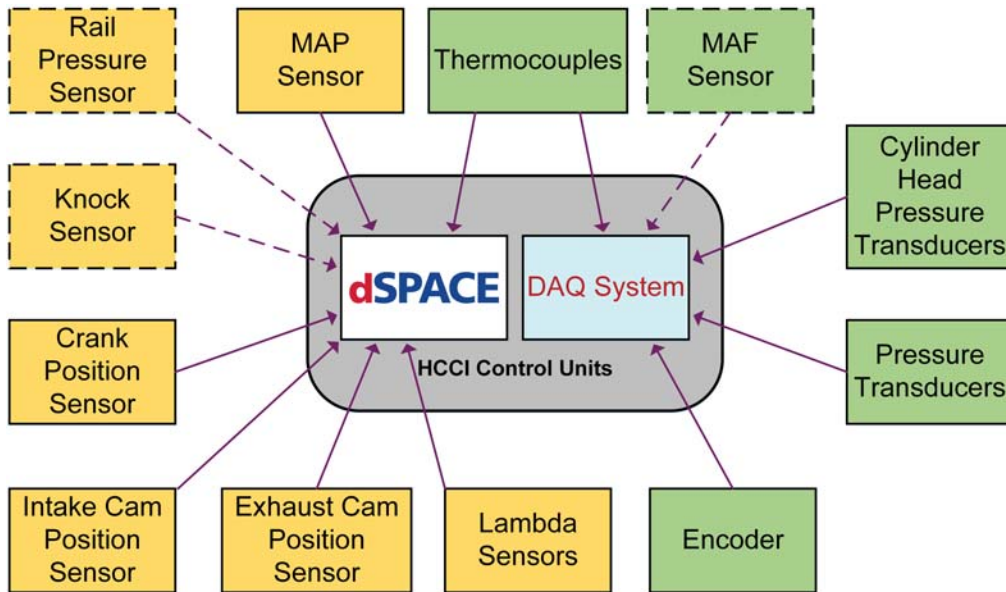


Figure 2.13: Engine Sensors and Controller Units. Dashed lines Show Planned Future Work.

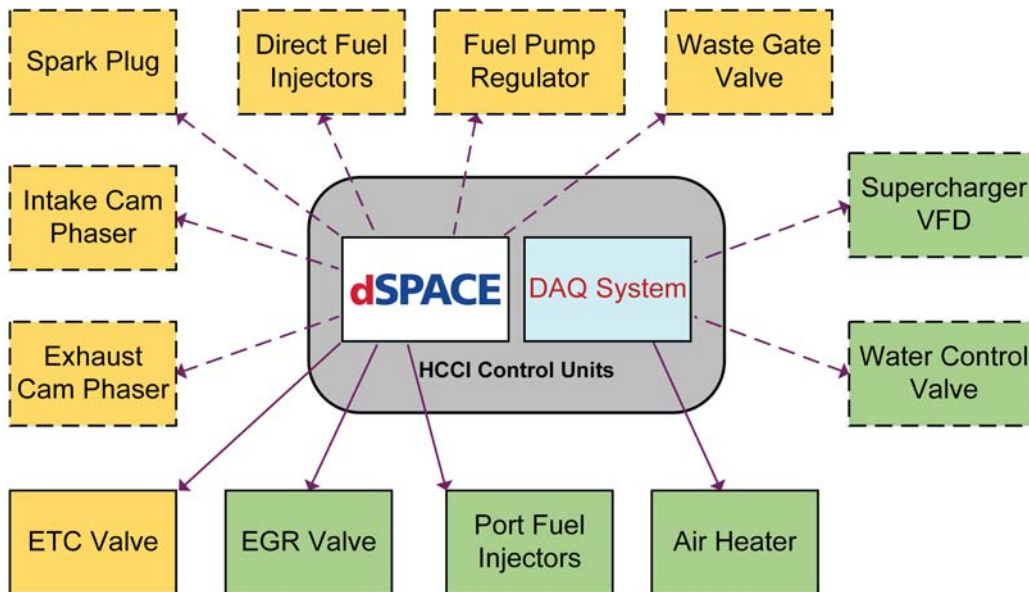


Figure 2.14: Engine Actuators and Controller Units. Dashed lines Show Planned Future Work.

Chapter 3

HCCI control oriented model

3.1 Control Oriented Model

A control oriented model (COM) is defined as a set of physics based equations that simulate the working of a physical system. Hence, the HCCI COM is a model developed based on its physics which simulates the working principles of an HCCI engine based on cycle by cycle variation. The HCCI COM described later in this chapter is an extension of a COM developed in [35], [36]. The new COM predicts CA50, T_{exh} and IMEP on cycle by cycle basis.

The COM is developed for a single cylinder Ricardo engine with the specifications listed in Table 3.1. For developing the COM for an HCCI engine, the engine cycle is divided into five parts including induction stroke, compression stroke, combustion period from start of combustion (SOC) to the end of combustion (EOC), expansion stroke, and exhaust stroke. Along with engine cycle equations, an empirical correlation [36] is used for predicting IMEP and a new physical model is developed for predicting exhaust gas temperature (T_{exh}).

Table 3.1
Ricardo Engine Specification

Bore	80 mm
Stroke	88.90 mm
Number of cylinders	1
Compression ratio	10 : 1
Displacement	447 cc
Number of valves	4
Intake valve opening	-175° aBDC
Intake valve closing	+55° aBDC
Exhaust valve opening	-70° aBDC
Exhaust valve closing	-175° aBDC

3.2 HCCI Engine Cycle Model

The HCCI model consists of a set of equations which describe the complete HCCI engine cycle from intake valve opening (IVO) to exhaust valve closing (EVC), i.e. describing the properties of air, fuel and residual gas mixture along with in-cylinder temperature and pressure throughout the cycle. Here the cycle starts with the air and fuel induction until the EVC. The index 'k' and index 'k+1' denote the previous cycle and present cycle respectively. Following sections include the thermodynamic formulas and empirical correlations to describe the COM for an HCCI engine cycle.

3.2.1 Induction Stroke

Pressure and temperature at intake valve closing (IVC), i.e. P_{ivc} and T_{ivc} , can be predicted using semi empirical correlations developed by Shahbakhti and Koch [37]. The following

two correlations are used to determine pressure and temperature at IVC:

$$P_{ivc,k+1} = \left[\frac{N_k^{a_1} \times \Phi_k^{a_2}}{T_{man,k}^{a_3}} \right] \times P_{man,k} \quad (3.1)$$

$$T_{ivc,k+1} = (b_1 \times T_{man,k}^2 + b_2 \times T_{man,k} + b_3) \left[\frac{\Phi_k^{c_1} \times N_k^{c_2}}{(1 + EGR)^{c_3}} \right] P_{man,k} \quad (3.2)$$

where P_{ivc} is in [kPa] and T_{ivc} in [$^{\circ}C$]. P_{man} , T_{man} , N , Φ and EGR are intake manifold pressure in [kPa], intake manifold temperature in [$^{\circ}C$], engine speed in [rpm], equivalence ratio and exhaust gas recirculation respectively. Constants a_1 , a_2 , a_3 , b_1 , b_2 , b_3 , c_1 , c_2 , and c_3 are 2.70e-2, 4.60e-2, 5.0e-3, -2.80e-3, 6.97e-1, 1.09e+2, -7.84e-2, -4.03e-2 and 3.20 e-3 respectively.

During the induction stroke, a fresh charge of air and fuel get mixed with the trapped residual gases from the previous cycle [36]. This mixing process has an impact on the temperature of the charge at IVC. Thus, a correlation is developed assuming ideal gas law and energy conservation principles which incorporate the mixing of residual gas with a fresh charge. A modified T_{ivc} denoted as T_{mix} is a better representation of the temperature of the mixture at the end of the induction stroke:

$$T_{mix,k+1} = (1 - RGF_k) \times \frac{C_{v,fc}}{C_{v,t}} \times T_{ivc,k+1} + RGF_k \times \frac{C_{v,rg}}{C_{v,t}} \times T_{rg,k} \quad (3.3)$$

T_{mix} is mixture temperature in [$^{\circ}C$] and RGF is the residual gas fraction. Subscript ' fc ' denotes fresh charge, ' rg ' denotes residual gases and ' t ' denotes total mixture. C_v is the average of gas specific heat capacity in (kJ/kg-K). $C_{v,fc}$ and $C_{v,rg}$ are 7.70e-1 (kJ/kg-K) and 8.180e-1 (kJ/kg-K) respectively and they are assumed to be constant during induction stroke.

3.2.2 Compression Stroke

After IVC, compression of air, fuel, and residual gas mixture takes place. From the point of IVC to SOC, this process can be assumed to be a polytropic process [38], so the mixture temperature and pressure at SOC are determined using the following equations:

$$T_{soc,k+1} = T_{mix,k+1} \left(\frac{V_{ivc,k+1}}{V_{soc,k+1}} \right)^{k_c-1} \quad (3.4)$$

$$P_{soc,k+1} = P_{ivc,k+1} \left(\frac{V_{ivc,k+1}}{V_{soc,k+1}} \right)^{k_c} \quad (3.5)$$

where P_{soc} is in [kPa] and T_{soc} in [K]. V_{ivc} and V_{soc} are the cylinder volume at IVC and SOC respectively. Cylinder volume at any instant is calculated by the sliding crank mechanism equation [38]. k_c is the specific heat capacity ratio during compression period and is determined using thermo-kinetic simulations [39].

3.2.3 Combustion Period

3.2.3.1 Start of Combustion (SOC) and CA50 Prediction

In the previous work of Shahbakhti and Koch [37], a modified knock integral model (MKIM) was developed for predicting SOC position for an HCCI engine. MKIM is accurate for predicting SOC but its highly nonlinear structures limits its use as a model for real time control [35]. Hence a simple fitted empirical correlation using MKIM was developed. This results in condensing MKIM to an empirical correlation. According to Shahbakhti [40] and Gozalic [41], the fuel's octane number, equivalence ratio and mixture

temperature and pressure at IVC are the major dominating factors for SOC prediction. Therefore, the following relation is used to predict SOC timing

$$\Theta_{soc,k+1} = f(T_{mix,k+1}, P_{ivc,k+1}, ON_{k+1}, \Phi_{k+1}) \quad (3.6)$$

where Θ_{soc} is the crank angle position at SOC. CA50 is calculated assuming a constant fuel burning rate:

$$\Theta_{CA50,k+1} = \Theta_{soc,k+1} + 0.5 \times \Delta\Theta_{comb,k+1} \quad (3.7)$$

where $\Delta\Theta$ is the difference between crank angle position from SOC to EOC. The CA50 also depends on the same dominating factors as SOC. Thus, the following relation is used:

$$\Theta_{CA50,k+1} = g(T_{mix,k+1}, P_{ivc,k+1}, ON_{k+1}, \Phi_{k+1}) \quad (3.8)$$

Fig.3.1 shows a comparison between detailed nonlinear MKIM and an empirical correlation for CA50 (Eq-3.8). MKIM is used for computing CA50 at 38896 different combinations of engine operating conditions shown in Table 3.2. Then MKIM data is used to parameterize the empirical correlation for predicting CA50:

$$\Theta_{CA50,k+1} = D_1 \cdot \Phi_k \cdot T_{mix,k+1} + D_2 \cdot P_{ivc,k+1} + D_3 \cdot \Phi_k + D_4 \cdot ON_k + D_5 \quad (3.9)$$

where constants D_1 , D_2 , D_3 , D_4 and D_5 are 0.617, -0.090, 224.121, 0.252 and 29.618. These values are obtained after fitting a correlation between $CA50_{MKIM}$ and CA50 from Eq-3.9. As the average error between $CA50_{MKIM}$ and predicted CA50 is 1.3 CAD, RMSE is 1.5 CAD, and the standard deviation is 1.1 CAD for all operating points, the CA50 correlation (Eq-3.9) is convincing for CA50 calculation. The steady state validation of the CA50 correlation with experimental data obtained from [28], is shown in Fig.3.2, the operating condition of the experimental data is shown in Table 3.3.

Table 3.2
Range of HCCI Engine Operating Conditions to Carry Out MKIM Simulations

Parameter	Range	Interval
T_{mix}	390 - 420 °C	2 °C
P_{ivc}	110 - 160 kPa	5 kPa
ON	0 - 40	2.5
Φ	0.3 - 0.6	0.025
N	1000	Constant
% EGR	0	Constant

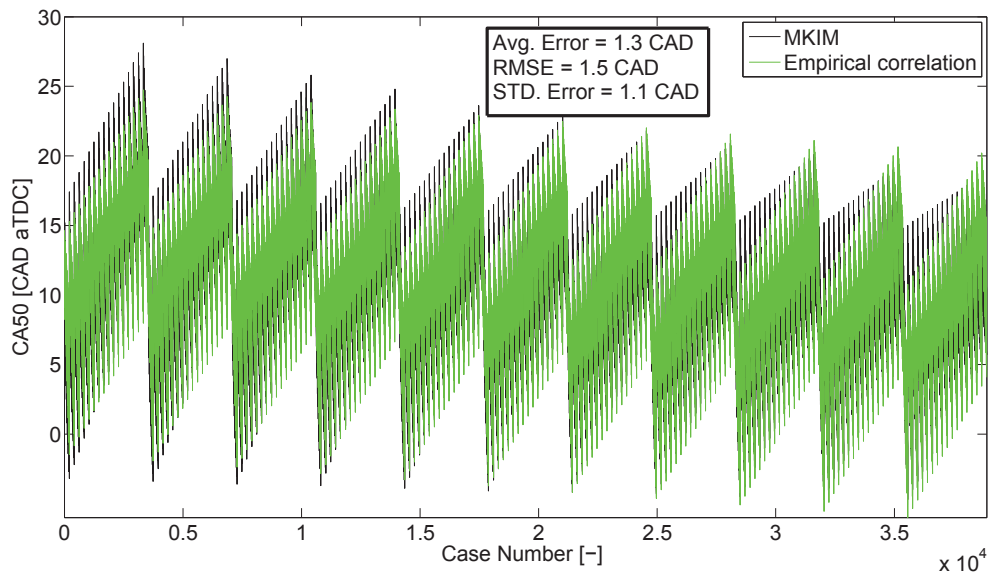


Figure 3.1: Comparison Between CA50 Prediction from MKIM and CA50 Correlation, RMSE Stands for Root Mean Square Error

Table 3.3
Operating Range of Experimental Data for Steady State Validation

Parameter	Range
ON	0 - 40
Φ	0.3 - 0.7
P_{man}	100 - 120 kPa
T_{man}	90 - 140 °C
N	900 - 1000 rpm

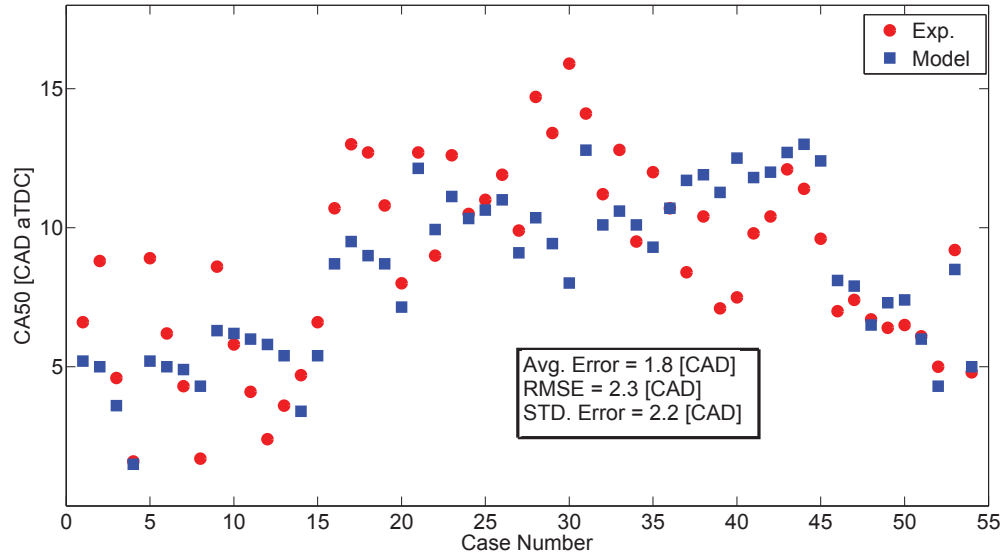


Figure 3.2: Steady State Validation for CA50 Correlation

3.2.3.2 End of Combustion (EOC)

The in-cylinder temperature at the EOC is calculated by applying the first law of thermodynamics from SOC to EOC. It is assumed that there is no heat loss during combustion from the walls to the cylinder because of the short burn duration. The first law of thermodynamics states that the internal energy at the EOC of the system is equal to the sum of internal energy U_{soc} at SOC, energy release Q_{fuel} by burned fuel, and work $W_{soc-eoc}$ performed from SOC to EOC. This yields:

$$U_{eoc} = U_{soc} + Q_{fuel} - W_{soc-eoc} \quad (3.10)$$

After substituting the empirical correlation for $W_{soc-eoc}$ from [42] and assuming the process of combustion to be adiabatic, the mixture temperature rise from SOC to EOC

is determined by using following correlation:

$$\Delta T_{comb} = \left(\frac{LHV_f \times CoC}{(1 + RGF_k)(\Phi_k^{-1} \times AFR_{st} + 1)C_v} \right) \quad (3.11)$$

where ΔT_{comb} is the rise in temperature due to combustion, LHV_f is the lower heating value of the blended fuel mixture (i.e. n-heptane and iso-octane), CoC is the average completeness of combustion, and AFR_{st} is the stoichiometric air-fuel ratio. LHV_f is calculated using the following formula,

$$LHV_f = \frac{(\%V_{nHep}\rho_{nHep}LHV_{nHep}) + (\%V_{iso}\rho_{iso}LHV_{iso})}{\%V_{nHep}\rho_{nHep} + \%V_{iso}\rho_{iso}} \quad (3.12)$$

where %V is volume percentage of fuel, ρ and LHV are the density and lower heating value of respective fuel ($\rho_{nHep} = 6.820e+2 \text{ kg/m}^3$, $\rho_{iso} = 6.900e+2 \text{ kg/m}^3$, $LHV_{nHep} = 4.456e+4 \text{ (kJ/kg)}$ and $LHV_{iso} = 4.434e+4 \text{ (kJ/kg)}$). The mixture temperature at EOC is obtained by using following equation:

$$T_{eoc,k+1} = T_{soc,k+1} + \Delta T_{comb} \quad (3.13)$$

The in-cylinder pressure at EOC in [kPa] is determined by using mass conservation law and ideal gas law between SOC and EOC:

$$P_{eoc,k+1} = \frac{P_{soc,k+1} \times V_{soc,k+1}}{V_{eoc,k+1}} \times \frac{T_{eoc,k+1}}{T_{soc,k+1}} \times \frac{R_{eoc}}{R_{soc}} \quad (3.14)$$

where the values for average gas constants R_{soc} and R_{eoc} are $2.890e-1 \text{ kJ/kg-K}$ and $2.893e-1 \text{ kJ/kg-K}$ respectively.

3.2.4 Expansion Stroke

From the point of EOC until exhaust valve opening (EVO), the process is assumed as a polytropic process [38]. Thus, the mixture temperature and pressure at EVO are estimated by the following equations:

$$T_{evo,k+1} = T_{eoc,k+1} \left(\frac{V_{eoc,k+1}}{V_{evo,k+1}} \right)^{k_e - 1} \quad (3.15)$$

$$P_{evo,k+1} = P_{eoc,k+1} \left(\frac{V_{eoc,k+1}}{V_{evo,k+1}} \right)^{k_e} \quad (3.16)$$

where P_{evo} is in [kPa], T_{evo} in [K], V_{eoc} and V_{evo} are the cylinder volume at EOC and EVO respectively. These volumes are calculated using the sliding crank mechanism equation. k_e is the polytropic constant during the expansion stroke.

3.2.5 Exhaust Stroke

The in-cylinder gas temperature at exhaust valve closing T_{evc} is assumed to be the same as the temperature of residual gases T_{rg} which get trapped inside the combustion chamber at the end of the cycle. The temperature of residual gases is estimated by assuming an isentropic relation during exhaust stroke [43]- [44]:

$$T_{rg,k+1} = T_{evo,k+1} \left(\frac{V_{evo,k+1}}{V_{evc,k+1}} \right)^{k_e - 1} \quad (3.17)$$

where T_{rg} is in [K], V_{evo} and V_{evc} are the cylinder volumes at EVO and EVC respectively.

$$m_{evc,k+1} = \frac{P_{exh} \times V_{evc,k+1}}{R_{evc} \times T_{rg,k+1}} \quad (3.18)$$

Pressure in exhaust manifold (P_{exh}) is assumed to be equal to atmospheric pressure. The mass of gas m_{evc} in [kg] remaining inside the cylinder at EVC are calculated using ideal gas law. The gas constant R_{evc} is equal to $2.893e-1$ kJ/kg-K. The RGF for the cycle is defined as the ratio of mass of residual gas remaining inside the cylinder at EVC to the total mass (m_t) of combustion mixture:

$$RGF_{k+1} = \frac{m_{evc,k+1}}{m_{t,k+1}} \quad (3.19)$$

3.3 Exhaust Gas Temperature Model

The COM developed up to now can give the in-cylinder gas temperature until the point of EVC. This section further extends the scope of the COM by adding a model for calculating the exhaust gas temperature before entering a catalytic converter. Fig.3.3 shows a schematic diagram for the flow of exhaust gases from the exhaust valve until the start of the catalytic converter. The following are the assumptions which are used for developing the exhaust gas temperature model.

1. The temperature of exhaust gases leaving the combustion chamber is equal to T_{evc} .
2. Heat transfer occurs only due to convection between the exhaust gases and the manifold as marked by red dashed lines in Fig.3.3. The remaining forms of heat transfer are included by a Q_{corr} term.
3. Temperature at point (A) in Fig.3.3 is assumed to be mean of T_{evc} and T_{exh} .
4. The surface temperature of exhaust manifold is constant and equal to ambient temperature ($T_{ambient}$).
5. Changes in kinetic and potential energy in the exhaust manifold are neglected.

The first law of thermodynamics is applied to the control volume in Fig.3.3. After rearranging the energy equation, the following formula is derived to calculate T_{exh} :

$$T_{exh} = \frac{hA_{surf}(T_{evc} - T_{surf}) + (\dot{m}_{exh}C_v - (hA_{surf}/2))T_{evc} + Q_{corr}}{\dot{m}_{exh}C_v + (hA_{surf}/2)T_{evc}} \quad (3.20)$$

where h is convective heat transfer coefficient in W/m^2-K , A_{surf} and T_{surf} are the surface

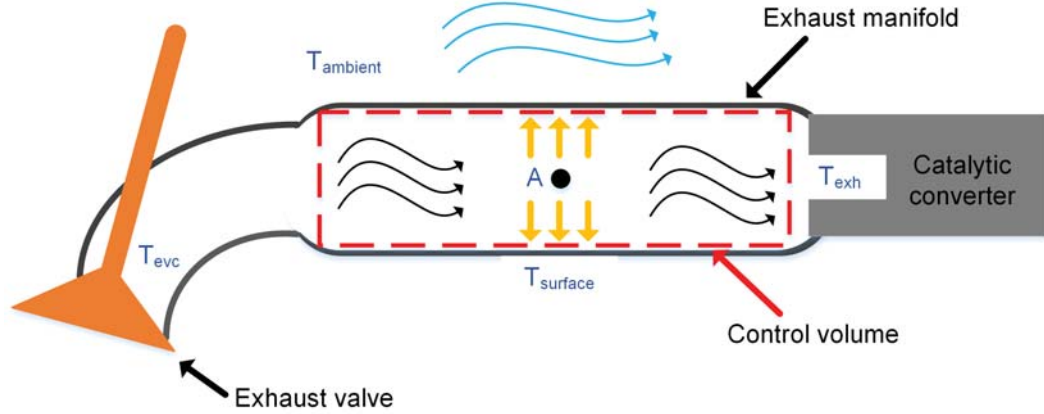


Figure 3.3: Schematic of the Control Volume for T_{exh} Model

area and surface temperature for the exhaust manifold respectively. Variable \dot{m}_{exh} is the mass flow rate of exhaust gases passing from the exhaust manifold. The values for the convective heat transfer coefficient and Q_{corr} are obtained after parameterizing the physical model equation with the experimental data from [28] for the Ricardo engine. The steady state validation of T_{exh} physical model is shown in Fig.3.4.

3.4 Indicated Mean Effective Pressure (IMEP) Model

The engine IMEP is calculated by using a physical model from [36]:

$$IMEP_{k+1} = m_{t,k+1} \cdot \frac{C_v}{V_{dis}} \cdot (T_{mix,k+1} - T_{soc,k+1} + T_{eoc,k+1} - T_{evc,k+1}) \quad (3.21)$$

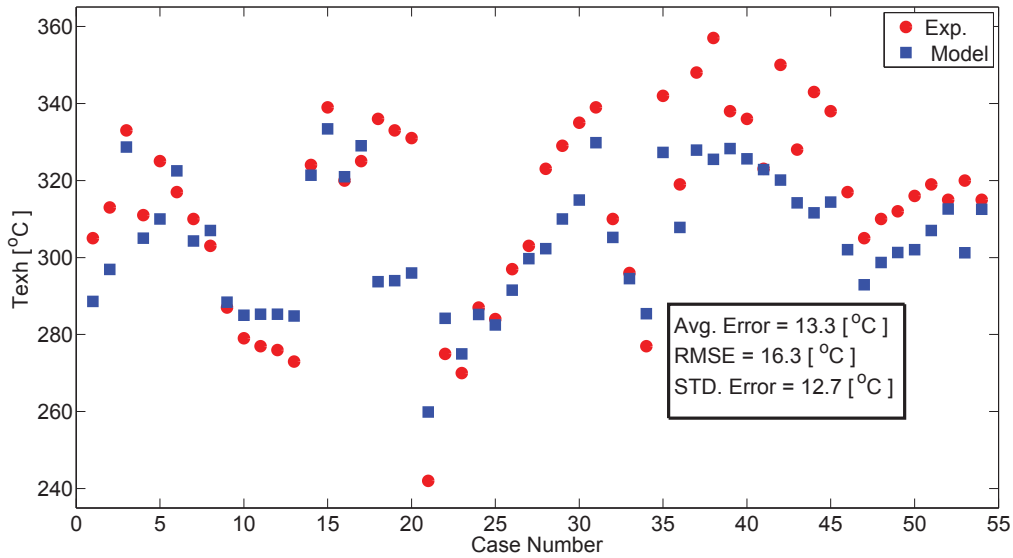


Figure 3.4: Steady State Validation for T_{exh} Physical Model

where IMEP is in [bar] and V_{dis} is the engine displacement volume in [m^3]. The steady state validation for the IMEP model with the experimental data from [28], is shown in Fig.3.5.

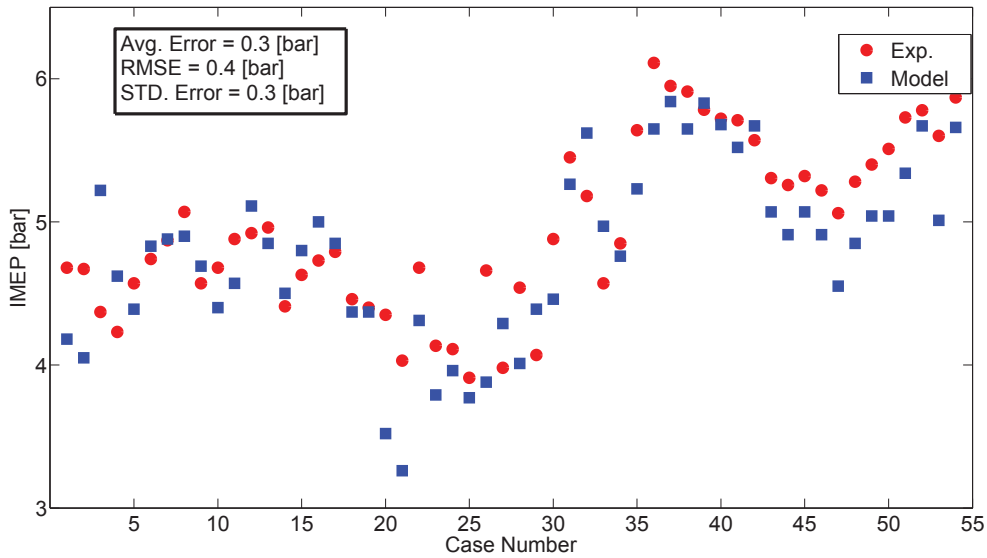


Figure 3.5: Steady State Validation for IMEP Model

3.5 Thermocouple Lag

A 1/32” sheathed J-type thermocouple was inserted in the exhaust manifold for measuring exhaust gas temperature during transient engine operations [29]. The thermocouple has a lag in responding to sudden exhaust gas temperature variations. This lag is accounted for by introducing a first order discrete lag model to the exhaust gas temperature model:

$$G(z) = \frac{0.05606}{z - 0.9439} \quad (3.22)$$

3.6 Transient Validation of COM

Performance of the COM is also tested at transient engine operating conditions. Fig.3.6 shows the comparison between experimental and simulated CA50, IMEP, and T_{exh} for a step change in ON and Φ . Other parameters including P_{man} , T_{man} , N, and EGR % were kept constant. Table 3.4 shows the accuracy of the COM for predicting CA50, IMEP and T_{exh} for the HCCI engine during the transient condition. Note that the accuracy is measured between experimental data and the COM predicted values. From Fig.3.6, it can be observed that the COM predictions are in very good agreement with the experimental data, therefore the COM can be used as a simulation test bed for designing real time model based HCCI controllers.

Table 3.4
Accuracy of the COM for the Transient Engine Operation in Fig.3.6

Parameter	Average error	Uncertainty	RMSE
CA50 (CAD)	1.5	± 1.8	1.9
IMEP (bar)	0.20	± 0.11	0.22
T_{exh} ($^{\circ}C$)	2.5	± 2.1	2.9

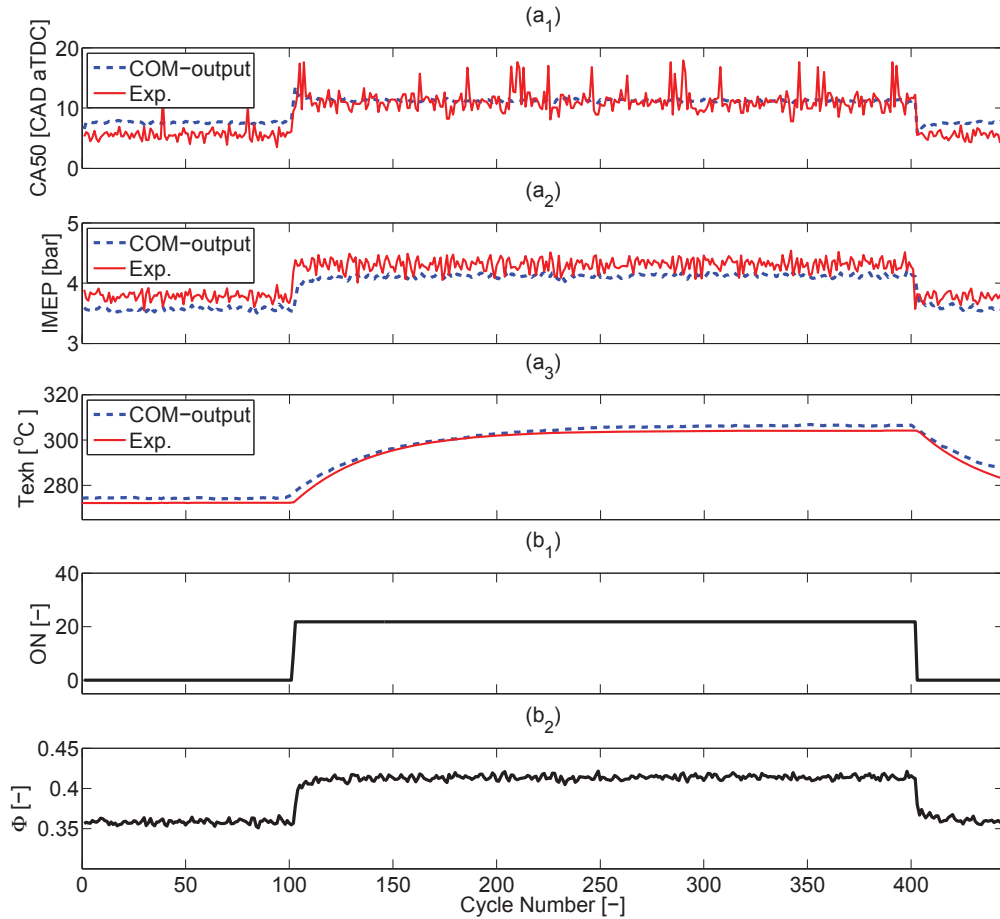


Figure 3.6: Validation of the COM for Transient Engine Operation. (a_x): Model and Experimental Data Comparison and (b_x): Inputs to the HCCI engine. P_{man} , T_{man} , N and % EGR are 110 kPa, 91 °C, 815 rpm and 0 % Respectively

3.7 Model Summary

By stepping through all the equations from [Eq-3.1] to [Eq-3.21], the COM is divided into three major parts. The first part is from [Eq-3.1] to [Eq-3.19] which simulates an HCCI engine cycle from IVO to EVC. The second part is for predicting exhaust gas temperature and finally the third part is a model for calculating IMEP. The COM from this chapter will be used in the next chapter to design model-based HCCI controllers.

Chapter 4

HCCI Controller Design

4.1 Introduction of Controllers

Among various challenges faced by HCCI engines, one of the most critical and vital challenges is to control combustion phasing. Because of the lack of any direct means to initiate combustion. Combustion phasing contributes to optimizing engine performance, thermal efficiency, and exhaust emissions [6]. Along with combustion phasing (i.e. CA50), control of engine load (i.e. IMEP) and exhaust gas temperature (T_{exh}) will help to optimize engine operating range and minimize exhaust emissions by affecting catalyst light-off time in the exhaust aftertreatment system. Thus, it is necessary to design effective and robust controllers to adjust three major engine parameters including CA50, IMEP, and T_{exh} . This will assist HCCI engines to move a step forward towards production with minimum calibration requirements.

There are various controllers that have been developed and studied earlier for HCCI engines. Control variables including CA50, IMEP, peak in-cylinder pressure (P_{max}),

and crank angle of peak pressure ($\Theta_{P_{max}}$) are some of the common target controlled variables. Fig.4.1 shows an overview of HCCI controllers in literature. HCCI controllers can be classified based on type of controller, control variable, and number of controlling parameters. The major classification of these controllers is explained next.

4.1.1 Single-Output vs. Multi-Output Controllers

Depending on the number of control outputs, there are three different categories of controllers: single-output, double-output, and triple-output. In a single-output controller, only one engine variable is controlled by using a single control input parameter. In the first group, CA50 is the most common variable which has been controlled, because it is a robust indicator of HCCI combustion [45]. References [35], [46], [47], [48] and [49] are some examples of CA50 control studies. The design of double and triple controllers can be complex because control of one variable can have impact on the other control variables, which either leads to a restriction in the operating range or causes discrepancy in the controller's performance. In the group of double-output controllers, two variables are controlled simultaneously. References [24], [36], [50], [51] and [52] are some examples of double controllers. Parameters such as CA50, IMEP, net mean effective pressure (NMEP), and P_{max} are among the common control variables. There are very few studies on triple HCCI control in the literature [53]. Triple control of the exhaust gas temperature along with combustion phasing and engine output work is necessary for development of HCCI engines as discussed in Chapter 1. This chapter attempts to address this necessity by designing triple controllers for an HCCI engine.

4.1.2 Empirical Controllers vs. Model-Based Controllers

Based on the structure of a controller type, HCCI controllers in literature are divided into two main groups including empirical and model-based controllers. Empirical controllers are defined as controllers which are developed without incorporating plant model's dynamics (e.g. PID controller [54] and PI controller [55]). Whereas model-based controllers are defined as those controllers which are developed based on control models incorporating an engine plant's dynamics. Discrete sub-optimal sliding mode controller (DSSMC) [36], model predictive controller (MPC) [46], and linear-quadratic regulator (LQR) [52], are some examples of model-based HCCI controllers.

HCCI Control		Control Variables		
		CA50, P_{max} , Θ_{Pmax} , IMEP, NMEP, Cyclic Variability, T_{exh}		
Controller Types	PI, PID, DSSMC, Feed forward, State feedback, Integral state feedback, MPC, LQR, Nonlinear Observer-based controller	Single Control	Double Control	Triple Control
		<ul style="list-style-type: none"> PI Control of Cyclic Variability [Hellstrom 2014] MPC Control of CA50 [Widd 2014] DSSMC Control of CA50 [Bidarvatan 2014] PI Control of CA50 [Ebrahimi 2013] Integral State Feedback Control of CA50 [Bidarvatan 2012] Nonlinear Observer-based Control of CA50 [Chaing 2010] DSSMC Control of T_{exh} [This work] 	<ul style="list-style-type: none"> Integral State Feedback and Feedforward Control of CA50 and IMEP and indirect Control of T_{exh} [Bidarvatan 2014] DSSMC and Integral State Feedforward Control of CA50 and IMEP [Bidarvatan 2013] Feed forward Control for P_{max} and Θ_{Pmax} [Schauer 2013] MPC Control of CA50 and NMEP [Erlie 2013] LQR Control of P_{max} and Θ_{Pmax} [Shaver 2004] DSSMC Control of CA50 and T_{exh} [This work] 	<ul style="list-style-type: none"> PID and PI Control of CA50, T_{exh} and IMEP [This work] DSSMC and PI Control of CA50, T_{exh} and IMEP [This work]

Figure 4.1: Control Background of the HCCI Engines in Literature

A collection of empirical and model-based single, double, and triple controllers, are developed in this chapter for controlling HCCI engine parameters, including CA50, T_{exh} , and IMEP. Discrete PID and PI controllers are designed as empirical controllers and a DSSMC is developed as a model-based controller. DSSMC is developed using the COM from Chapter 3. The COM is linearized around a nominal HCCI operating point, shown in Table 4.1. This operating point is selected based on the Ricardo HCCI engine experimental results in [37] to ensure the operating point is located near the engine optimal region with minimal cyclic variations.

Table 4.1
Nominal Operating Point Around Which the Nonlinear COM is Linearized

Parameter	Value
CA50	10 CAD aTDC
T_{soc}	520°C
P_{soc}	2364 kPa
T_{rg}	365°C
m_{evc}	0.0347 g
RGF	6.3 %
ON	20
\dot{m}_{fuel}	0.097 g/cycle
P_{man}	125 kPa
T_{man}	110°C
N	1000 rpm
T_{exh}	300°C
External EGR	0 %

The HCCI experimental results from [28] and [42] show that blend fuel ratio (i.e. fuel ON), intake manifold pressure, and air fuel ratio are effective parameters to adjust CA50, T_{exh} , and IMEP, respectively. Therefore, ON, P_{man} and \dot{m}_{fuel} are selected as control inputs for the Ricardo HCCI engine.

4.2 Controller Test Bed

An experimentally validated, detailed physical HCCI engine plant model [37], is used as a test bed for controllers in this chapter. This model is bound to certain range of operating conditions for which the model has been parameterized [36]. Table 4.2 shows the range of input parameters for which the model is valid to use.

Table 4.2
Range of Input Parameters for the HCCI Plant Model

Parameter	Range
ON	0 - 40
Φ	0.36 - 0.48
P_{man}	100 - 140 kPa
T_{man}	90 - 148 °C
N	850 - 1050 rpm

4.2.1 Single-Input Single-Output (SISO) Controllers

Two SISO controllers are developed to control CA50 and T_{exh} independently. Controller types include PID and DSSMC. Engine parameters including T_{man} , N, %EGR, and \dot{m}_{fuel} are kept constant and equal to nominal operating values as listed in Table 4.1.

4.2.1.1 Discrete PID Controller for CA50

A discrete PID controller is designed to adjust the ON of fuel for tracking a desired trajectory of CA50. Structure of the SISO PID controller is shown in Fig.4.2. This controller works on the basis of the difference between the desired and actual CA50 values.

For the initial phase, the Ziegler and Nicholas close loop method [56] is used for finding the initial values of gains. The obtained gain values are $K_p = 0.7$, $K_i = 1400$, and $K_d = 0.002$. These gain values are then manually tuned to $K_p = 1.3$, $K_i = 2500$, and $K_d = 0.01$ for optimum controller performance. Fig.4.3 shows the tracking performance of the PID controller for both positive and negative step changes in CA50.

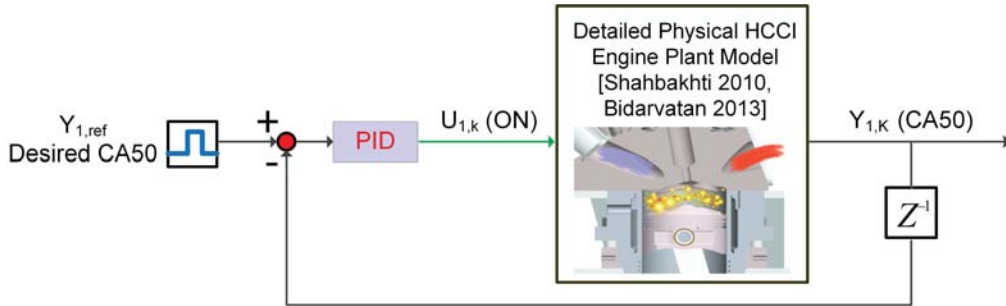


Figure 4.2: Structure of CA50 PID Controller

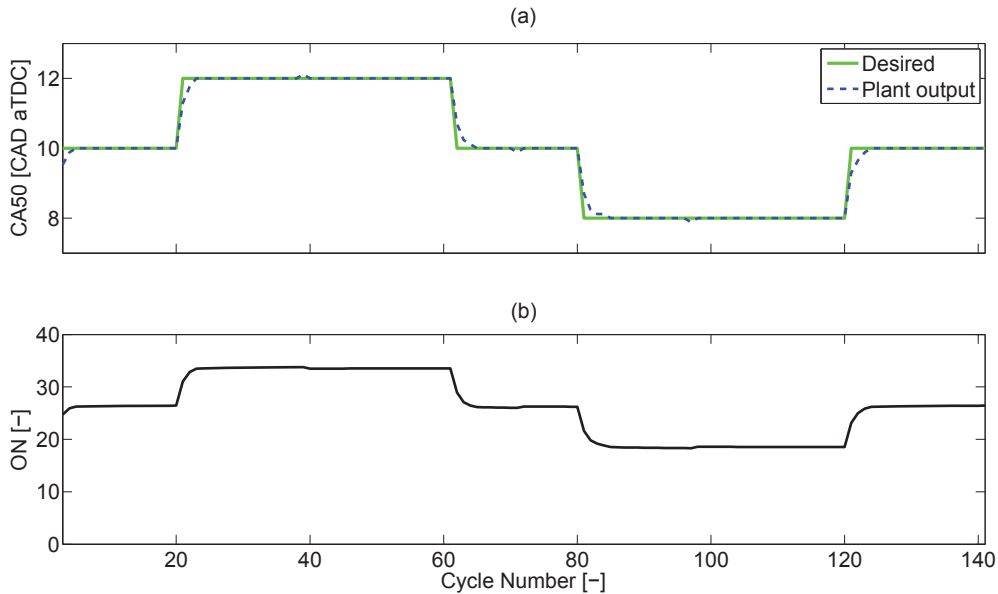


Figure 4.3: Tracking Performance of CA50 PID Controller. (a): Plant Output and (b): Control Input

4.2.1.2 Discrete PID Controller for T_{exh}

Similar to CA50 PID controller, a SISO PID controller is developed to control T_{exh} by adjusting the intake manifold pressure (P_{man}). Fig.4.4 shows the structure of the T_{exh} PID controller.

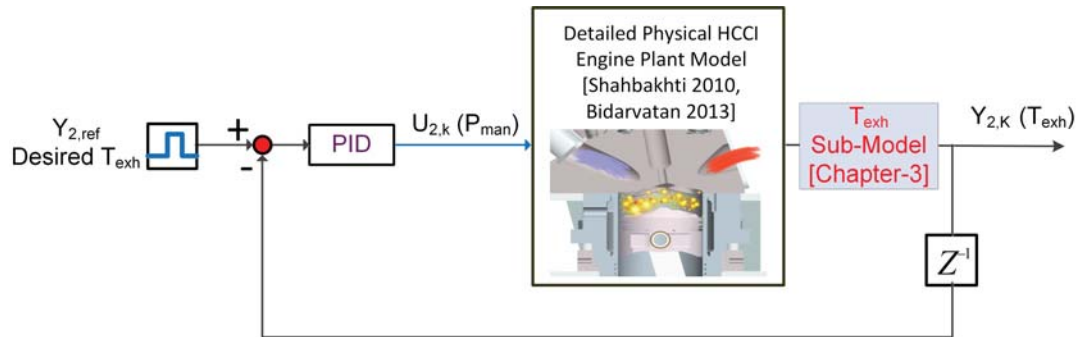


Figure 4.4: Structure of T_{exh} PID Controller

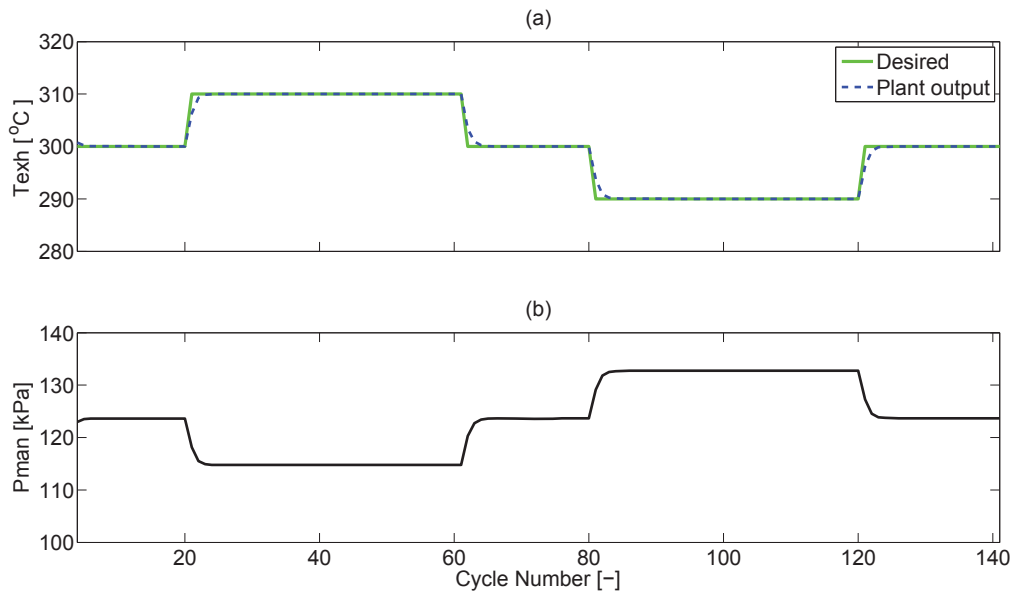


Figure 4.5: Tracking Performance of T_{exh} PID Controller. (a): Plant Output and (b): Control Input

The gain values obtained from the Ziegler and Nicholas close loop method are $K_p = 0.2$, $K_i = 0.400$, and $K_d = 0.0003$. These gain values are then manually tuned to $K_p = 0.65$, $K_i = 600$, and $K_d = 0.001$ for obtaining the optimal performance of the controller. Fig.4.5 shows the tracking performance of the controller for both positive and negative step changes in the desired T_{exh} .

4.2.1.3 DSSMC for CA50

To develop a DSSMC, the first step is to get a state space model for the COM by linearizing it around the nominal operating point (Table 4.1). The system of equations for the linear state space model is:

$$x_{k+1} = A_1 x_k + B_1 u_{1,k} \quad (4.1)$$

$$y_{1,k} = C_1 x_{1,k} \quad (4.2)$$

where x is the state vector of the model, u_1 is the input to the plant model, and y_1 is the output of the model. Index ' $k + 1$ ' and ' k ' denote current and previous engine cycles, respectively. For designing DSSMC of CA50, five states are selected [36] including $x = [CA50 \ T_{soc} \ P_{soc} \ T_{rg} \ m_{evc}]^T$. Input u_1 is ON and the output y_1 is CA50. After linearizing the COM for these five states, the following state space matrices are obtained:

$$A_1 = \begin{bmatrix} 0.024 & -0.006 & 0.002 & -0.021 & -140.8 \\ -0.034 & 0.008 & -0.002 & 0.030 & 201.9 \\ -0.425 & 0.108 & -0.036 & 0.370 & 2484 \\ 0.140 & -0.035 & 0.012 & -0.044 & -818.6 \\ -7.6e^{-6} & 1.95e^{-6} & -6.55e^{-7} & -2.44e^{-6} & 0.0446 \end{bmatrix}$$

$$B_1 = \begin{bmatrix} 0.289 \\ -0.498 \\ -6.139 \\ 0.7289 \\ 3.9e^{-5} \end{bmatrix}$$

$$C_1 = \begin{bmatrix} 1 & 0 & 0 & 0 & 0 \end{bmatrix}$$

Poles of the system are -0.0173, 0.0155, -0.0020, 0 and 0. Since the poles are within the unit circle, the system is stable for the selected operating point. After developing the state space model, the next step is to design a state observer which can estimate the model state variables. A Luenberger state estimator [57] is designed to estimate the five states which are not easily measurable in an HCCI engine. The estimated model states (\hat{x}_{k+1}) are based on the previous cycle states (\hat{x}_k), the estimated outputs ($\hat{y}_{1,k}$), and disturbance ($w_{k,1}$). The equation for designing the Luenberger estimator is as follows:

$$\hat{x}_{k+1} = A_1 \hat{x}_k + B_1 u_{1,k} + E w_{k,1} + l_1 (y_{1,k} - \hat{y}_{1,k}) \quad (4.3)$$

where E represents disturbance matrix and l_1 is the Luenberger gain vector which can be estimated using a pole placement technique [57]. For DSSMC of CA50 the best estimated Luenberger gain vector is:

$$l_1 = \begin{bmatrix} 0.1629 \\ -2.9301 \\ -91.7526 \\ -0.2194 \\ -0.0012 \end{bmatrix}$$

From the observer, the estimated states are then transferred to the DSSMC, which regulates the control input (ON) based on the desired output (CA50) trajectory. The DSSMC works

on a principle of discrete linear quadratic regulator sub-optimal control law for determining and driving the system to a control sliding surface [36]. Assume the sliding surface of CA50 DSSMC is $S_{slid,1}$. The equations for finding the sliding surface for designing DSSMC are as follows [58]:

$$S_{slid,1} = \begin{bmatrix} G & 1 \end{bmatrix} T \quad (4.4)$$

where T and G are found by the following equations:

$$TB_1 = \begin{bmatrix} 0_{n-m \times 1} \\ M_{m \times m} \end{bmatrix} \quad (4.5)$$

$$G = R - P \quad (4.6)$$

where M is any non singular matrix which satisfies the Eq.(4.5). Variables n and m are the model states and number of control inputs, respectively (here $n=5$ and $m=1$). R can be determined solving Riccati cartesian equation and P is found using the following method:

$$Q = (T^{-1})^T D T^{-1} = \begin{bmatrix} Q_{11} & Q_{12} \\ Q_{21} & Q_{22} \end{bmatrix} Q_{11} \varepsilon \mathfrak{R}^{n-m \times n-m} Q_{12} \varepsilon \mathfrak{R}^{n-m \times m} Q_{21} \varepsilon \mathfrak{R}^{m \times n-m} Q_{22} \varepsilon \mathfrak{R}^{m \times m} \quad (4.7)$$

where D is a constant, positive definite, and symmetrical matrix.

$$P = -Q_{21} Q_{22}^{-1} \quad (4.8)$$

The procedure for solving Riccati cartesian equation [36] for finding R is as follows:

$$TAT^{-1} = \begin{bmatrix} a_{11} & a_{12} \\ a_{21} & a_{22} \end{bmatrix} \quad (4.9)$$

$$a^o = a_{11} - a_{12}(Q_{22}^{-1})^T Q_{21}^T \quad (4.10)$$

$$b^o = a_{12} \quad (4.11)$$

$$c^o = Q_{11} - Q_{12}(Q_{22}^{-1})^T Q_{21}^T \quad (4.12)$$

$$d^o = Q_{22} \quad (4.13)$$

$$e^o = (a^o)^T [e^o - e^o b^o ((b^o)^T e^o d^o b^o + d^o)^{-1} (b^o)^T e^o] a^o + c^o \quad (4.14)$$

$$R = ((b^o)^T e^o b^o + d^o)^{-1} (b^o)^T e^o a^o \quad (4.15)$$

The sliding surface obtained for CA50 DSSMC is a vector of 1×5 matrix (i.e. $S_{slid,1} = [0.0075 \ -0.0129 \ -0.1592 \ 0.0189 \ -0.1328]$). Hence, the control input (u_1) from the DSSMC is determined by using the following equation [59]:

$$u_{1,k} = -(S_{slid,1} B_1)^{-1} [S_{slid,1} A_1 x_k + S_{slid,1} E w_{k-1,1}] \quad (4.16)$$

The first term in Eq.(4.16) is for regulating input and the second term is for disturbance rejection. In order to further enhance the tracking performance of the DSSMC, a feedforward gain (N_u) is added to the control structure as shown in Fig.4.6. Variable N_u can be calculated using the following correlation [57]:

$$\begin{bmatrix} N_x \\ N_u \end{bmatrix} = \begin{bmatrix} A_1 - I_n & B_1 \\ C_1 & 0 \end{bmatrix}^{-1} \begin{bmatrix} 0_{n \times 1} \\ I_m \end{bmatrix} \quad (4.17)$$

where I_m and I_n are the identity matrix of size m and n respectively and $0_{n \times 1}$ is the zero vector of size n . The value of N_u is determined to be 3.6023 after solving Eq.(4.17). The final form of control input can be rearranged as follows:

$$u_{1,k} = -(S_{slid,1}B_1)^{-1} [S_{slid,1}A_1x_k + S_{slid,1}Ew_{k-1,1}] + N_u y_{1,ref} \quad (4.18)$$

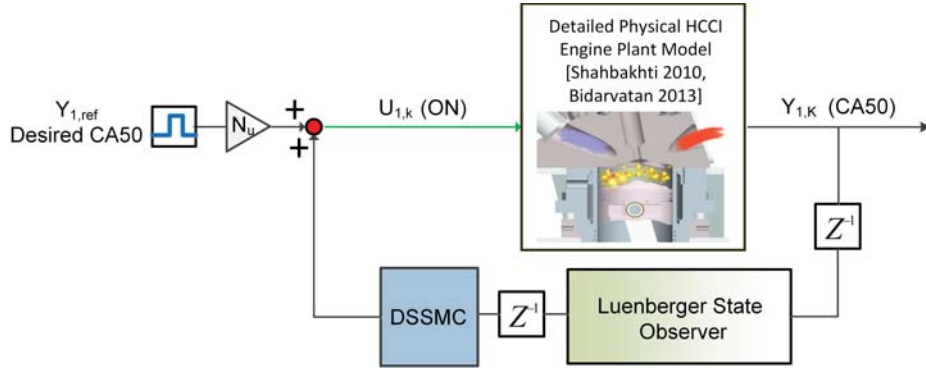


Figure 4.6: Structure of CA50 DSSMC

Fig.4.7 shows the tracking performance of the DSSMC for both positive and negative step changes of CA50.

4.2.1.4 DSSMC for T_{exh}

Similar to the DSSMC of CA50, all steps are followed for developing DSSMC of T_{exh} using P_{man} as the control input. Fig.4.8 shows the structure of the DSSMC for T_{exh} . A state space model is obtained after linearizing the COM around the nominal operating point. The equations for representing the state space model are as follows:

$$x_{k+1} = A_2x_k + B_2u_{2,k} \quad (4.19)$$

$$y_{2,k} = C_2x_{2,k} \quad (4.20)$$

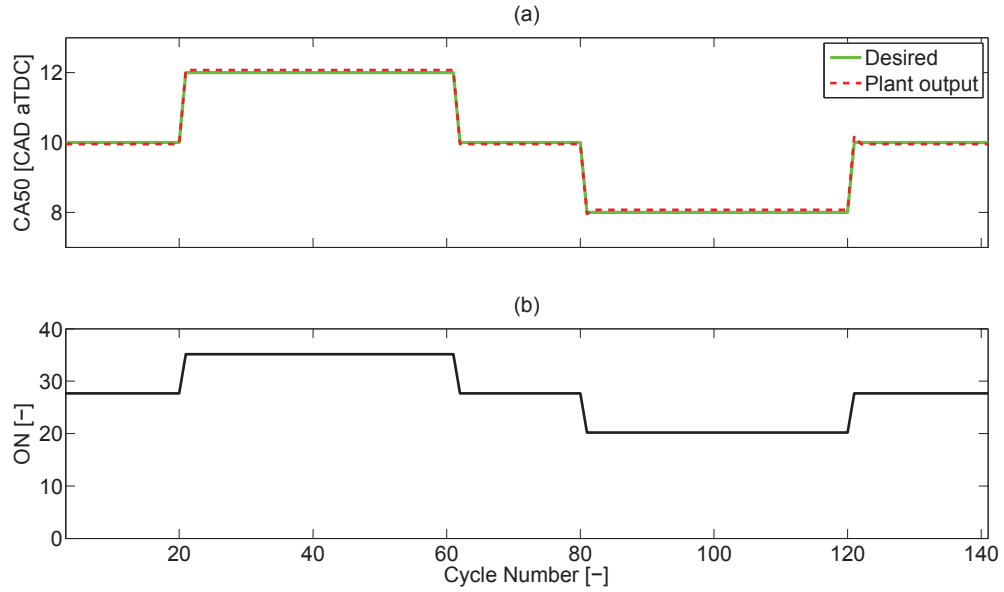


Figure 4.7: Tracking Performance of CA50 DSSMC. (a): Plant Output and (b): Control Input

The selected model states are $x = [T_{evc} \text{ CA50 } T_{soc} P_{soc} m_{evc}]^T$, input u_2 is P_{man} and output y_2 is T_{evc} . State T_{evc} correlates to T_{exh} by using the exhaust gas temperature model developed in Chapter 3. After linearizing the COM around the nominal operating point, the following state space matrix is obtained:

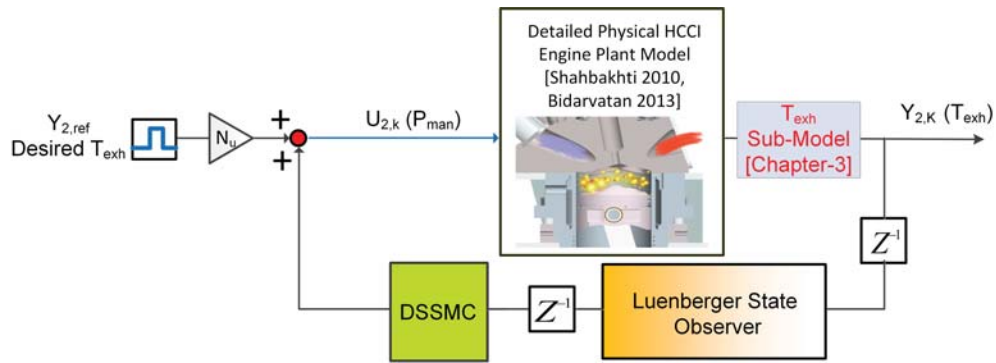


Figure 4.8: Structure of T_{exh} DSSMC

$$A_2 = \begin{bmatrix} -0.044 & 0.140 & -0.035 & 0.012 & -818.6 \\ -0.021 & 0.024 & -0.006 & 0.002 & -140.8 \\ -0.030 & -0.034 & -0.008 & -0.002 & 201.9 \\ 0.370 & -0.425 & 0.108 & -0.0365 & 2484 \\ -2.44e^{-6} & -7.6e^{-6} & 1.95e^{-6} & -6.55e^{-7} & 0.0446 \end{bmatrix}$$

$$B_2 = \begin{bmatrix} -1.826 \\ -0.015 \\ -0.164 \\ 14.1 \\ 3.7e^{-4} \end{bmatrix}$$

$$C_2 = \begin{bmatrix} 1 & 0 & 0 & 0 & 0 \end{bmatrix}$$

The poles of the system include -0.0176, 0.0154, -0.0016, 0, and 0. All the poles are within a unit circle, thus the system is stable for the selected operating point. The Luenberger gain vector obtained for the state space model is as follows:

$$l_2 = \begin{bmatrix} -0.0034 \\ -0.0139 \\ -0.0199 \\ 0.2449 \\ 0 \end{bmatrix}$$

The equations for estimating the states and adjusting P_{man} are as follows:

$$\hat{x}_{k+1} = A_2 \hat{x}_k + B_2 u_{2,k} + E w_{k,2} + l_2 (y_{2,k} - \hat{y}_{2,k}) \quad (4.21)$$

$$u_{2,k} = -(S_{slid,2}B_2)^{-1} [S_{slid,2}A_2x_k + S_{slid,2}Ew_{k1,2}] + Nu y_{2,ref} \quad (4.22)$$

The values of the sliding surface for T_{exh} DSSMC are $S_{slid,2}=[0.009 \ -0.00001 \ -0.0008 \ 0.0697 \ 0.1659]$. The value of feedforward gain (Nu) is equal to -0.5331 . Fig.4.9 shows the tracking performance of the T_{exh} DSSMC for both positive and negative step changes of the desired T_{exh} .

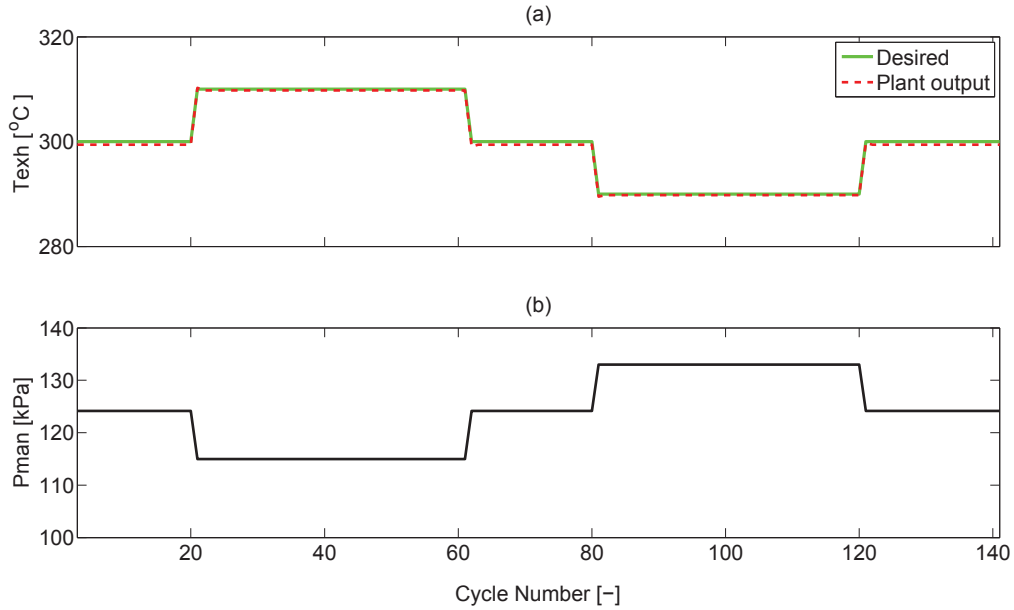


Figure 4.9: Tracking Performance of T_{exh} DSSMC. (a): Plant Output and (b): Control Input

The tracking performance of all SISO controllers are summarized in Table 4.3. It is been observed that for both SISO PID controllers the overshoot and steady-state error is equal to zero, whereas for DSSMCs there is less overshoot and steady state error (i.e. 0.2 CAD overshoot and 0.1 CAD steady state error). The reason for the steady state error is due to difference between the COM and the physical plant model. The rise time is equal to 1 cycle for both DSSMC SISO controllers. The settling times for the PID controllers are significantly slower compared to those from the DSSMCs.

Table 4.3
Tracking Performance For Designed SISO Controllers

Performance paramters	PID CA50	PID T_{exh}	DSSMC CA50	DSSMC T_{exh}
Rise time	2 cycles	2 cycles	1 cycle	1 cycle
Steady-state error	0 CAD	0°C	0.1 CAD	0.6°C
Maximum overshoot	0 CAD	0°C	0.2 CAD	0.2°C
Settling time	3 cycles	3 cycles	1 cycle	1 cycle

4.2.2 Two-Input Two-Output Controller

After developing SISO controllers for both CA50 and T_{exh} , they are combined to test the SISO controllers to adjust both combustion phasing and exhaust gas temperature, while keeping other engine parameters including T_{man} , \dot{m}_{fuel} , N, and %EGR constant and equal to their nominal values.

4.2.2.1 Discrete PID Controllers for CA50 and T_{exh}

The discrete PID controllers from section 4.2.1.1 and 4.2.1.2 are combined together as shown in Fig.4.10 to develop a multi-input multi-output (MIMO) control structure. Here, similar to previous controllers, CA50 is controlled by ON of fuel and T_{exh} is controlled by intake manifold pressure (P_{man}).

Fig.4.11 and Fig.4.12 show the tracking performance of the two-input two-output PID controller. Fig.4.11 is during single-output variable changing, and Fig.4.12 is when both variables are changing simultaneously. Results show that there is a good disturbance rejection capability for both individual controllers. The maximum steady-state deviation is 0 CAD and 0°C for tracking CA50 and T_{exh} , respectively. Thus, the impact of change in control input of each controller on the output of the other controller is completely

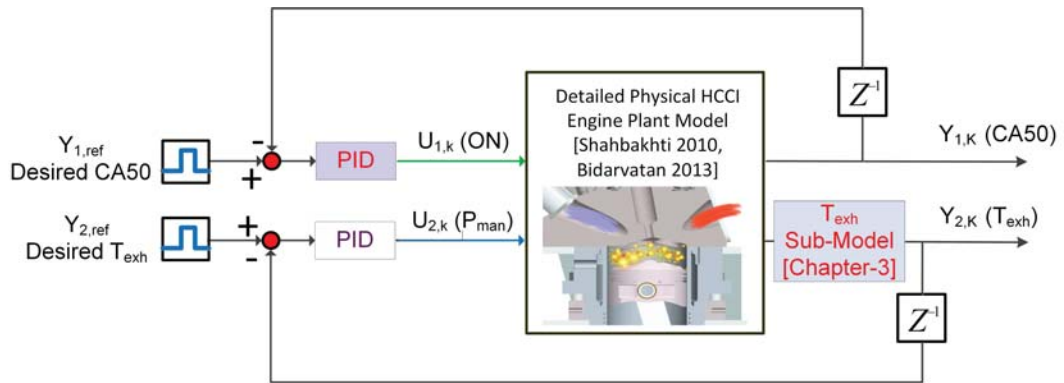


Figure 4.10: Structure of the MIMO PID Controller to Control CA50 and T_{exh}

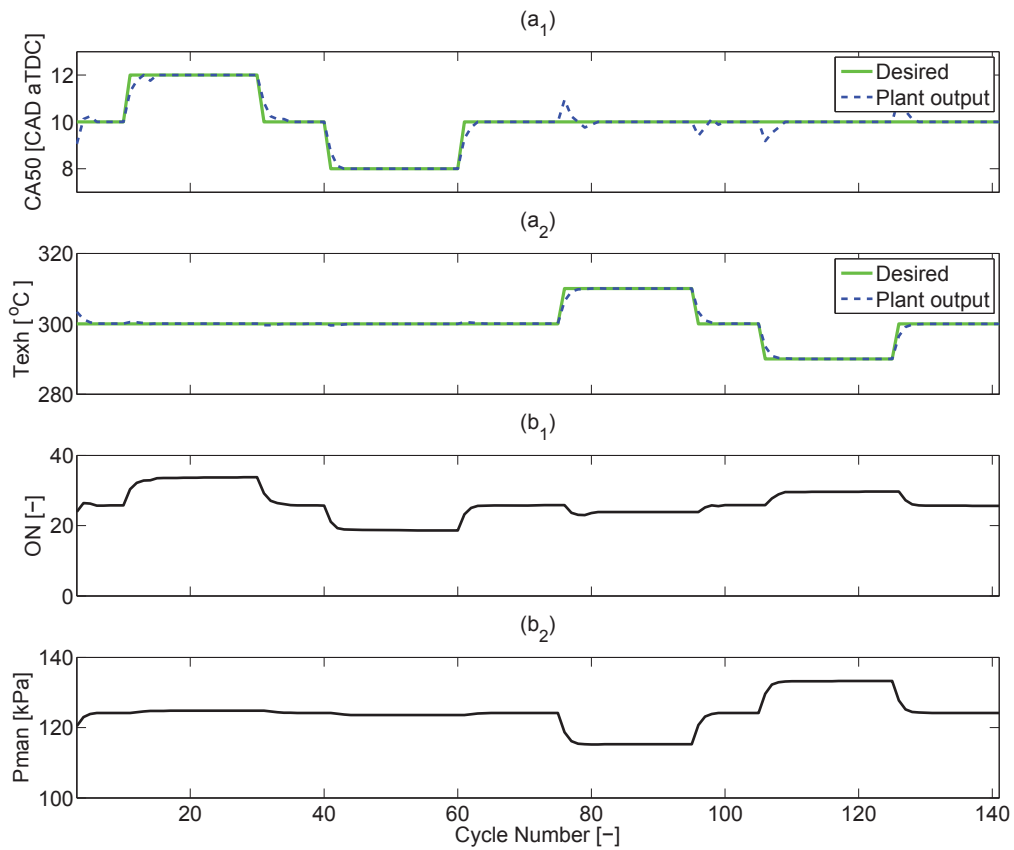


Figure 4.11: Single Tracking Performance of CA50 and T_{exh} by PID Controllers. (a_x): Plant Outputs and (b_x): Control Inputs

compensated.

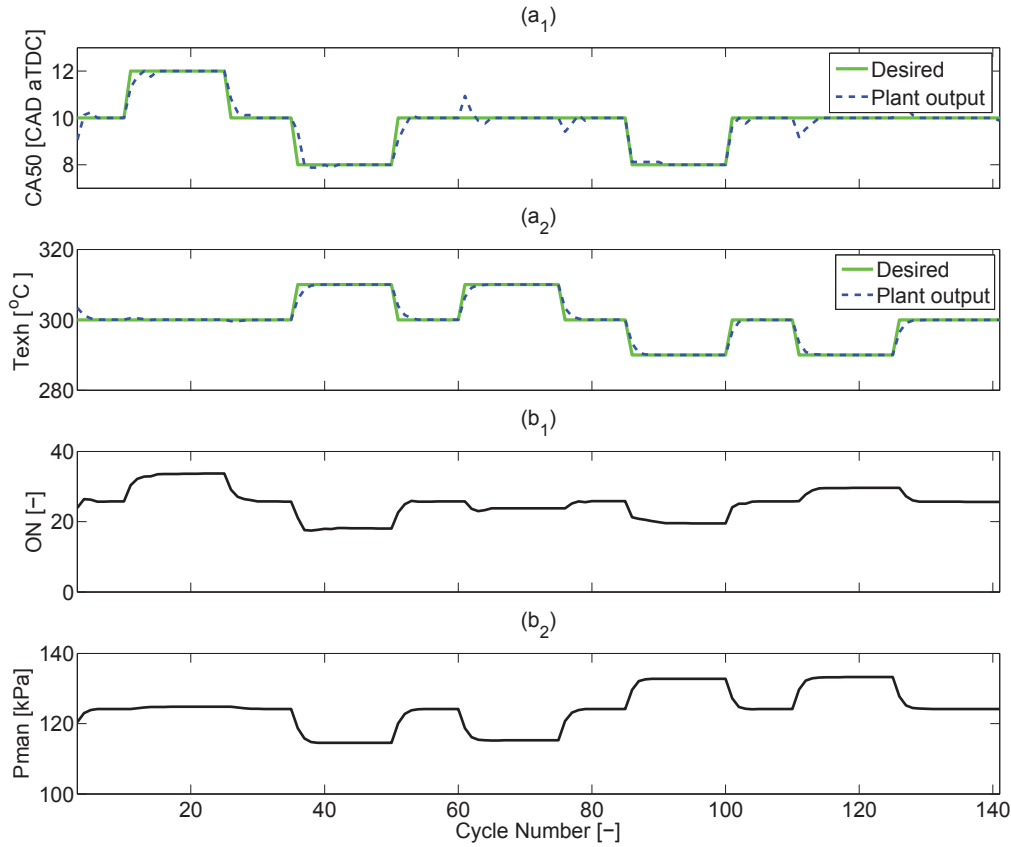


Figure 4.12: Simultaneous Tracking Performance of CA50 and T_{exh} by PID Controllers. (a_x): Plant Outputs and (b_x): Control Inputs

4.2.2.2 DSSMCs for CA50 and T_{exh}

Similar to the two-input two-output PID controller, both DSSMCs from section 4.2.1.3 and 4.2.1.4 are combined together to develop a model-based MIMO controller to adjust CA50 and T_{exh} simultaneously. Fig.4.13 shows the structure of a two-input two-output DSSMC. As the input of one controller affects the output of the other controller, a disturbance matrix is incorporated while designing both the observer and the DSSMC. In Fig.4.13, $W_{1,k}$ and $W_{2,k}$ are the disturbances caused by a change in ON and P_{man} , respectively. The values of error matrix for both CA50 and T_{exh} DSSMCs controllers are represented as E_1 and E_2 . The values of E_1 and E_2 matrices are shown as follows:

$$E_1 = \begin{bmatrix} 0.15 \\ 15.56 \\ -0.03 \\ -11.5 \\ 4e-4 \end{bmatrix}$$

$$E_2 = \begin{bmatrix} 0.73 \\ 0.29 \\ -0.5 \\ -1.14 \\ 0 \end{bmatrix}$$

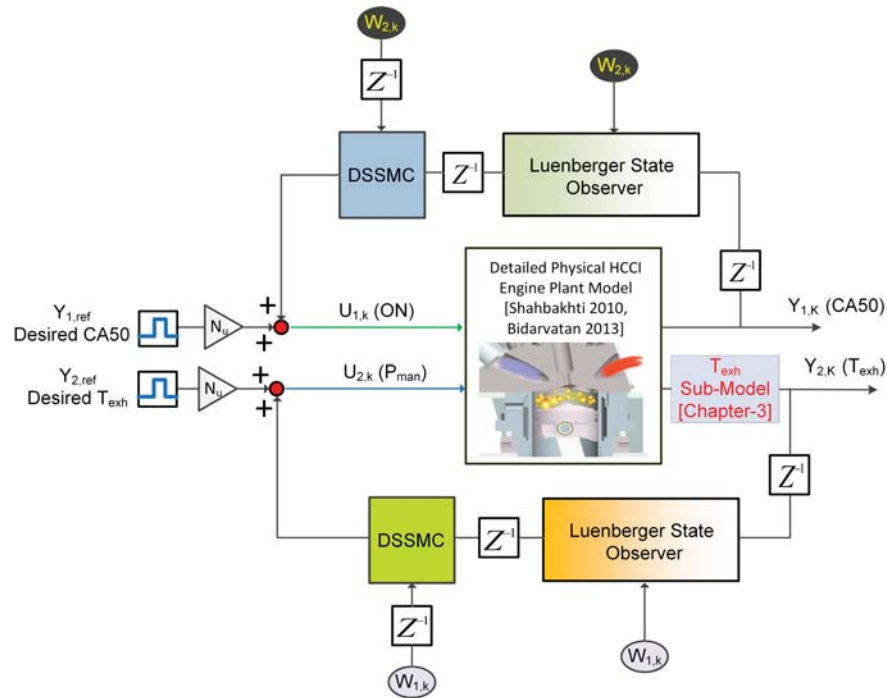


Figure 4.13: Structure of the MIMO DSSMCs to Control CA50 and T_{exh} . W_1 and W_2 are the Disturbance Simulated using the Plant Model

Fig.4.14 and Fig.4.15 show the tracking performance of the two-input two-output DSSMC during single and simultaneous change of output variables, respectively. The results show

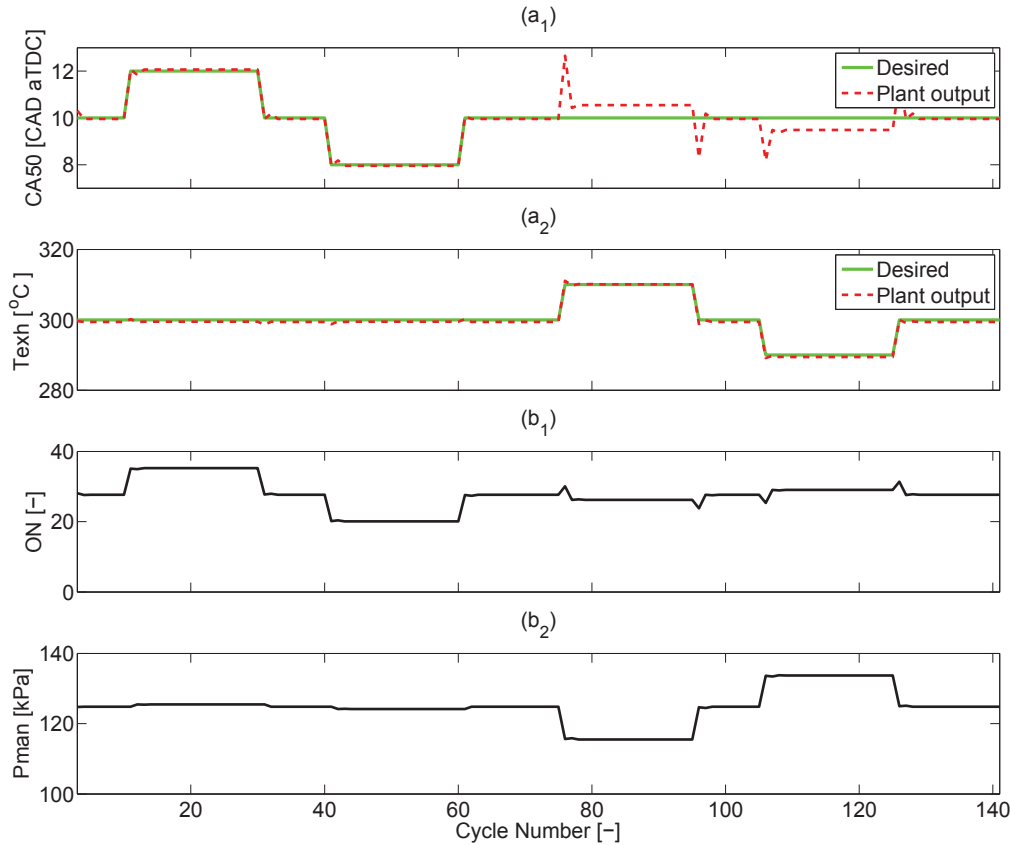


Figure 4.14: Single Tracking Performance of CA50 and T_{exh} by DSSMCs. (a_x): Plant outputs and (b_x): Control inputs

that CA50 DSSMC is not very accurate in rejecting the disturbance caused by P_{man} (the input variable of T_{exh} DSSMC). This is because of the model mismatch between the COM and the physical plant model. T_{exh} DSSMC accurately tracks the desired T_{exh} trajectory.

4.2.3 Comparisons of Two-Input Two-Output Controllers

Table 4.4 shows the tracking performances and the disturbance rejection performance of the two-input two-output controllers. It is observed that the response time for tracking the desired trajectory is faster in the DSSMC compared to the PID controllers. The number of cycles required for the PID controller to track a step change in CA50 and T_{exh} is equal to

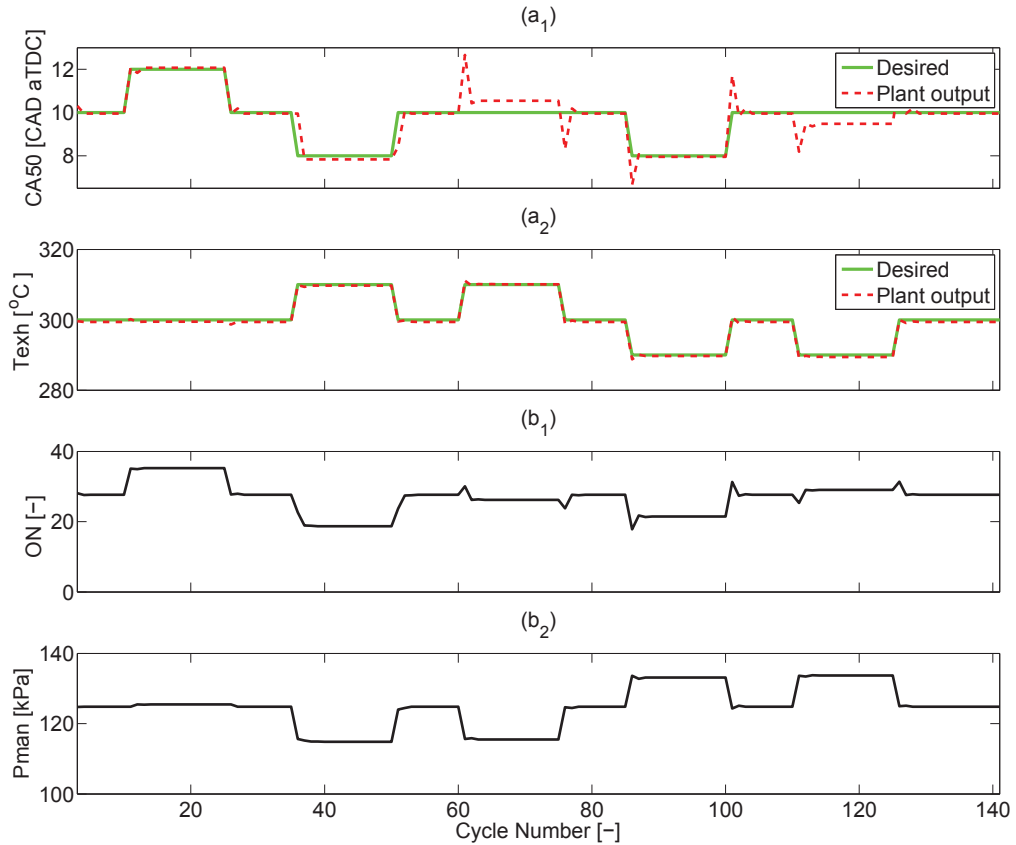


Figure 4.15: Simultaneous Tracking Performance of CA50 and T_{exh} by DSSMCs. (a_x): Plant Outputs and (b_x): Control Inputs

5 cycles and 3 cycles, respectively. Whereas for the DSSMCs it is 3 cycles and 2 cycles, respectively. There is some overshoot in T_{exh} DSSMC, but the steady-state error for both T_{exh} PID and T_{exh} DSSMC is equal. From the disturbance rejection point of view both CA50 and T_{exh} DSSMC can reject the disturbance with less cycles as compared to the PID controllers. But CA50 DSSMC has maximum steady-state deviation of 0.5 CAD because of the change in P_{man} , whereas in the case of the PID controller, it is 0 CAD.

Table 4.4
Tracking and Disturbance Rejection Performance of Two-Input
Two-Output Controllers

Performance paramters	PID controllers		DSSMCs	
	CA50	T_{exh}	CA50	T_{exh}
Rise time	3 cycles	2 cycles	1 cycle	1 cycle
Steady-state error	0 CAD	0°C	0.1 CAD	0°C
Maximum overshoot	0 CAD	0°C	0.1 CAD	1.1°C
Settling time	5 cycles	3 cycles	3 cycles	2 cycles
Dist. max. absolute deviation	1.1 CAD	3.9°C	2.6 CAD	1.1°C
Max. steady-state deviation	0 CAD	0°C	0.5 CAD	0.5°C
Dist. rejection speed	6 cycles	4 cycles	2 cycles	3 cycles

4.3 Three-Input Three-Output Controller

For integral control of the HCCI engine, a third controller is added for controlling IMEP. As \dot{m}_{fuel} has a direct impact on IMEP, it is selected as an input parameter for adjusting IMEP. A PI controller is designed for controlling IMEP. The initial tuned gain values for the PI controller are obtained from Ziegler and Nicholas close loop method. The gain values include $K_p = 0.003$ and $K_i = 6.04$ which are then further manually tuned to $K_p = 0.009$ and $K_i = 12$ for optimum performance of the PI controller. Other engine parameters including T_{man} , N and %EGR are kept constant and equal to their nominal values.

Fig.4.16 and Fig.4.17 show the schematic of the designed three-input three-output controllers termed as ‘Controller A’ and ‘Controller B’, respectively. Given that the new controller uses one more input variable (\dot{m}_{fuel}) for IMEP control) compared to the double-output controllers; it is more challenging to control the three engine parameters against disturbances caused by the two other sub-controllers, i.e. P_{man} and \dot{m}_{fuel} for CA50 DSSMC controller and ON and \dot{m}_{fuel} for T_{exh} DSSMC controller. The values disturbance matrices, E_1 and E_2 matrices are shown as follows:

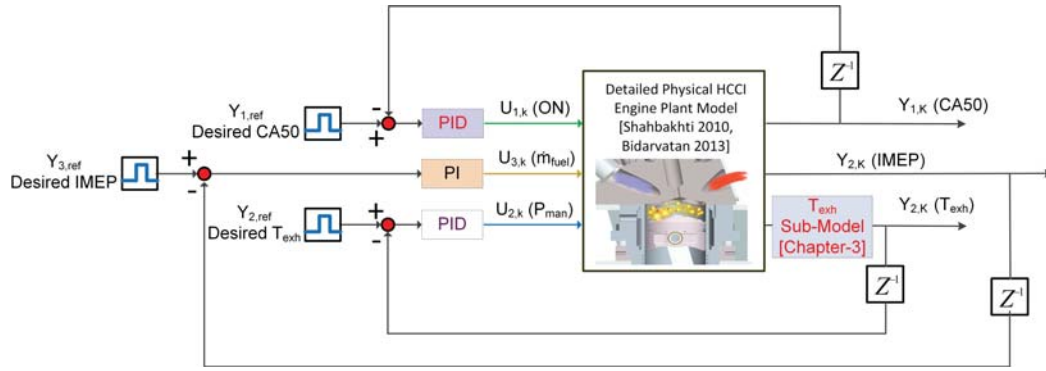


Figure 4.16: Controller A - Structure of MIMO Empirical Controller to Control CA50, T_{exh} and IMEP

$$E_1 = \begin{bmatrix} 0.15 & -158.9 \\ 15.56 & 197.2 \\ -0.03 & 1000 \\ -11.5 & 2184 \\ 4e-4 & -0.12 \end{bmatrix}$$

$$E_2 = \begin{bmatrix} 0.73 & -10500 \\ 0.29 & 10000.9 \\ -0.5 & 197.2 \\ -1.14 & -9000 \\ 0 & -0.12 \end{bmatrix}$$

The outputs from both MIMO controllers are compared with each other as shown in Fig.4.18 and Fig.4.19 for single and simultaneous variables changes, respectively. Fig.4.20 and Fig.4.21 shows the error between desired value and actual plant output for controller A and controller B for both single and simultaneous tracking, respectively. The tracking performance and disturbance rejection performance of both controllers are compared in Table 4.5. Since the same IMEP controller is added to both controllers, all the performance parameters for that IMEP PI controller are the same. The DSSMCs are found to respond

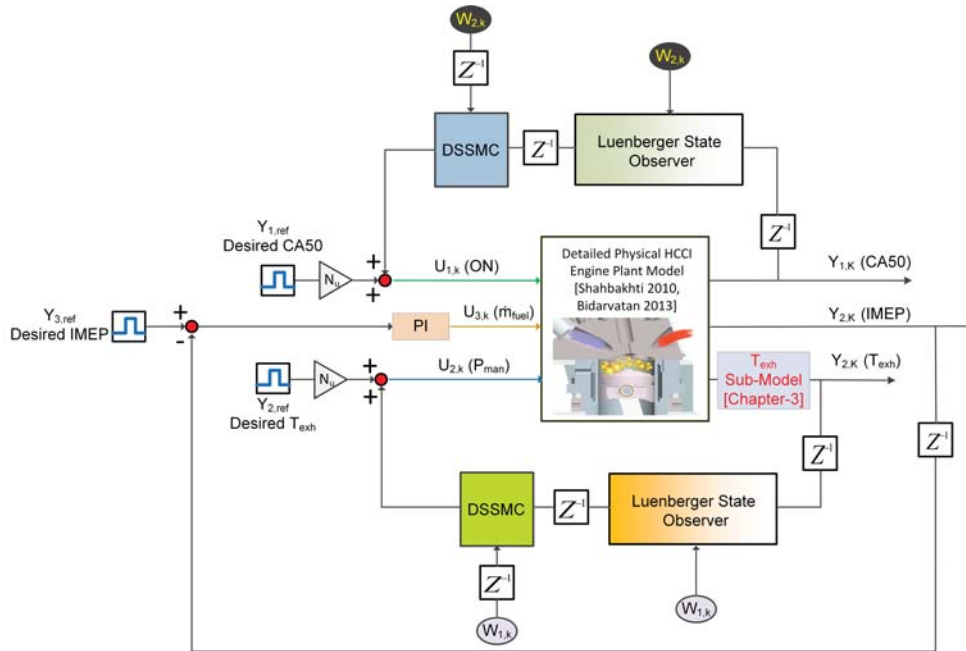


Figure 4.17: Controller B - Structure of Combined MIMO Model-Based / Empirical Controller to Control CA50, T_{exh} and IMEP. W_1 and W_2 are the Disturbance Simulated using the Plant Model

faster compared to the PID controllers, i.e. settling time for CA50 and T_{exh} for DSSMC are 3 cycles and 2 cycles, respectively, whereas for the PID controllers it is 6 cycles and 3 cycles, respectively. In addition, the disturbance rejection speed for DSSMCs are faster than that of the PID controllers.

The maximum steady-state error for CA50 and T_{exh} in DSSMCs of Controller B are higher than those in the PID controllers of Controller A. As previously mentioned, higher steady-state errors are due to model mismatch between the COM and the physical plant model.

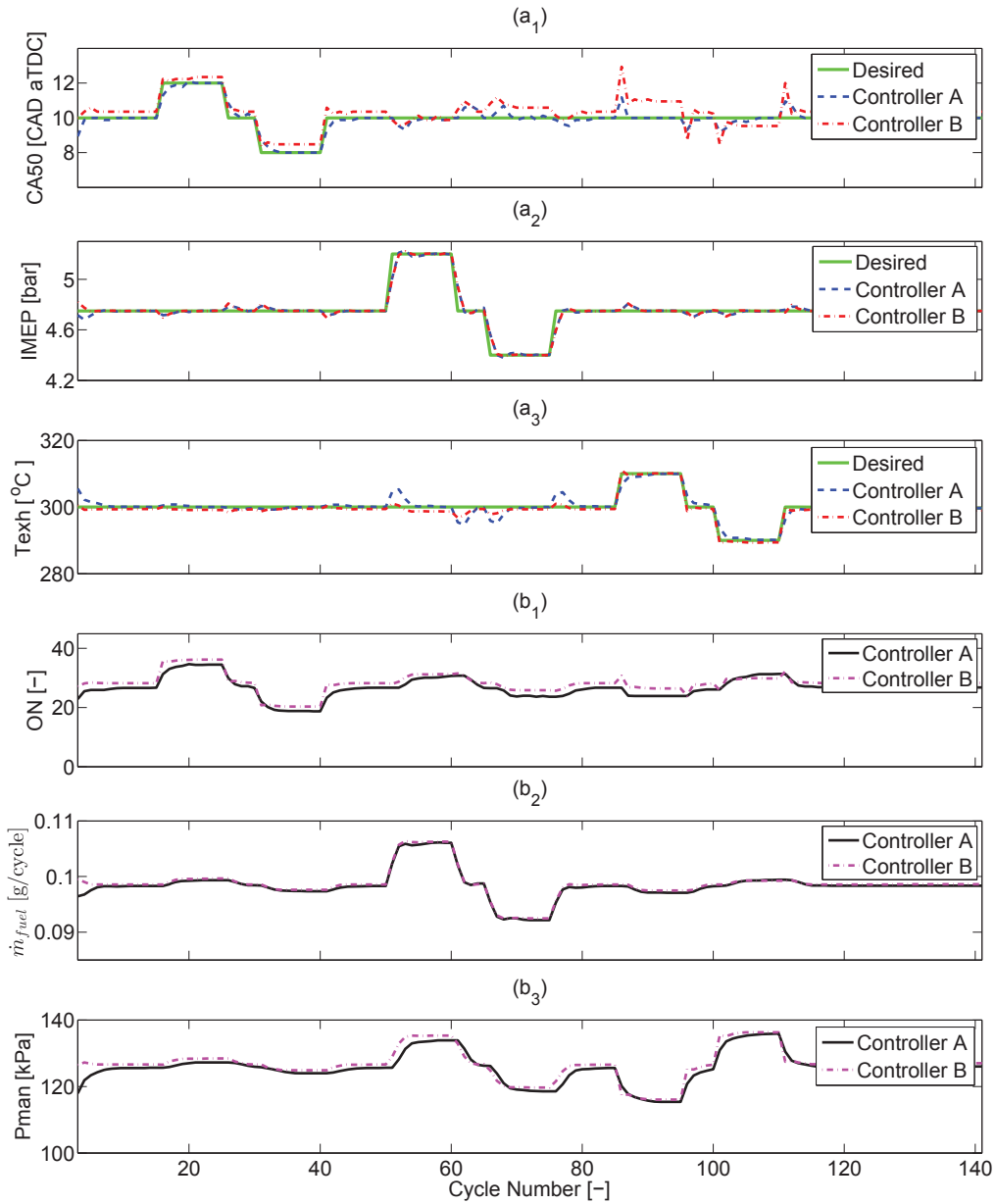


Figure 4.18: Comparing Single Tracking Performance for Three-Input Three-Output, Type A (Fig.4.16) and Type B (Fig.4.17) Controllers. (a_x): Plant Outputs and (b_x): Control Inputs

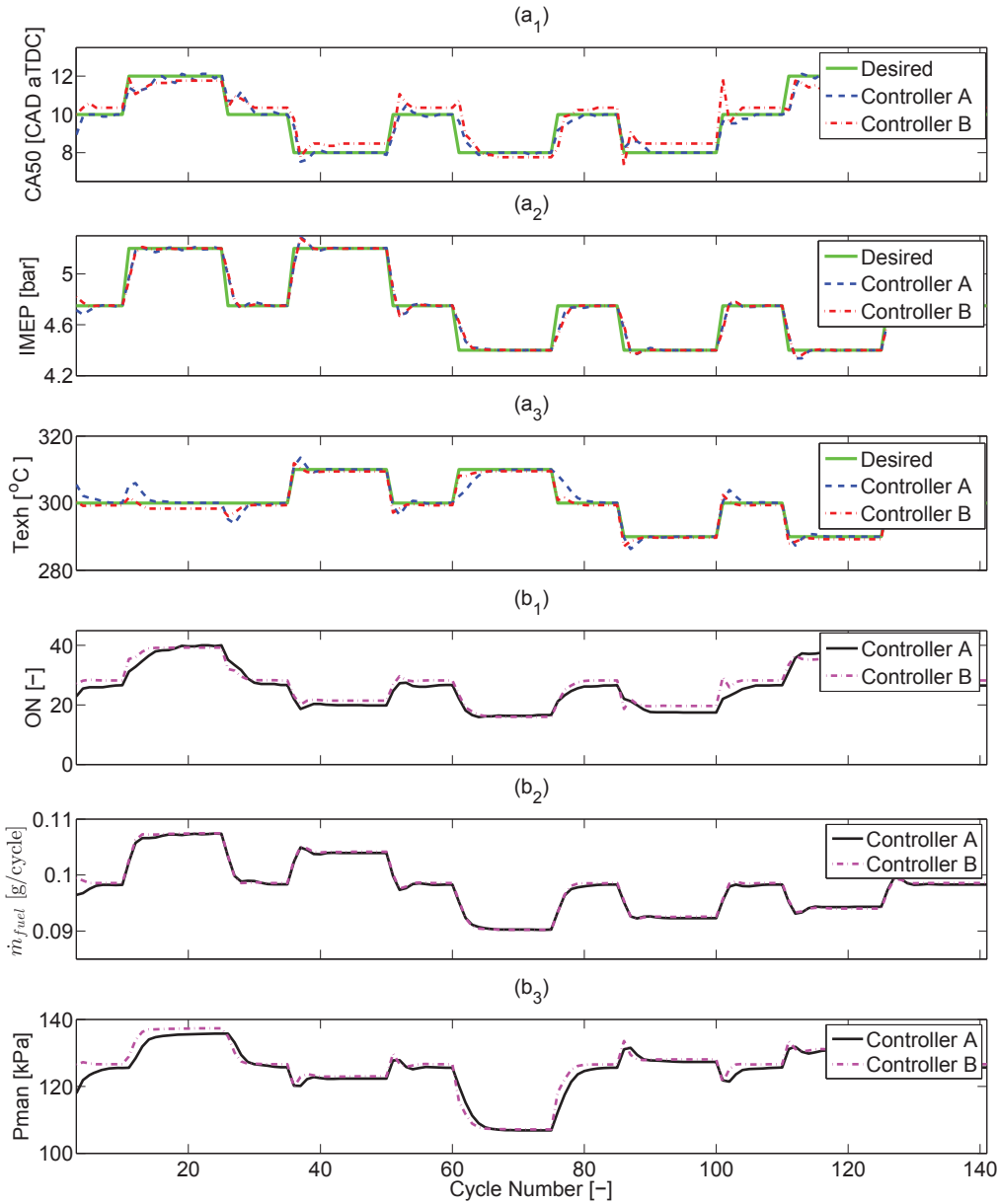


Figure 4.19: Comparing Simultaneous Tracking Performance for Three-Input Three-Output, Type A (Fig.4.16) and Type B (Fig.4.17) Controllers. (a_x): Plant Outputs and (b_x): Control Inputs

4.4 Controllers' Summary

Different empirical and model-based controllers were tested on the detailed physical HCCI plant model [42]. The simulated results show that all the PID controllers have almost

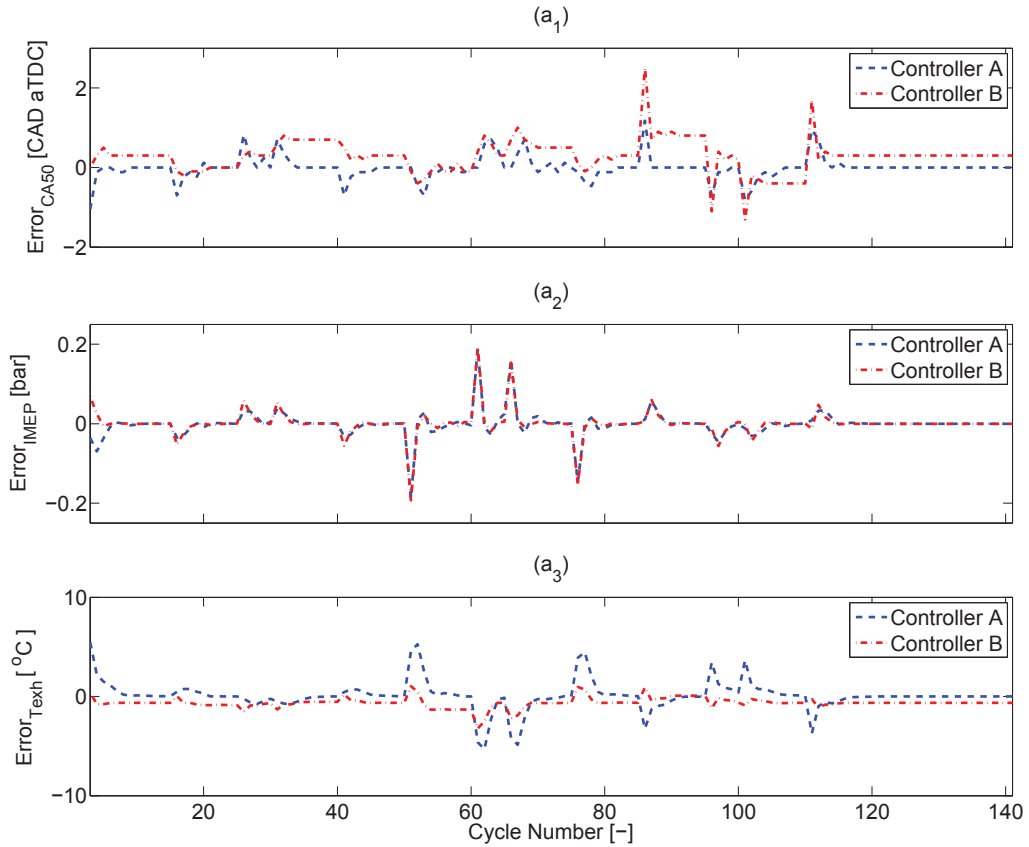


Figure 4.20: Tracking Error Comparison for Three-Input Three-Output, Type A (Fig.4.16) and Type B (Fig.4.17) Controllers for the Single Tracking Changes, where (a_x) are the Plant Outputs

zero overshoot and zero steady-state error, but the response time for rejecting disturbance and the settling time are slower than those of the model-based DSSMC. Because of the mismatch between the linearized state space matrix developed using the COM and the detailed physical HCCI plant model [36], the developed DSSMCs exhibited steady-state tracking errors of 0.1 CAD and 0.1 °C for CA50 and T_{exh} , respectively.

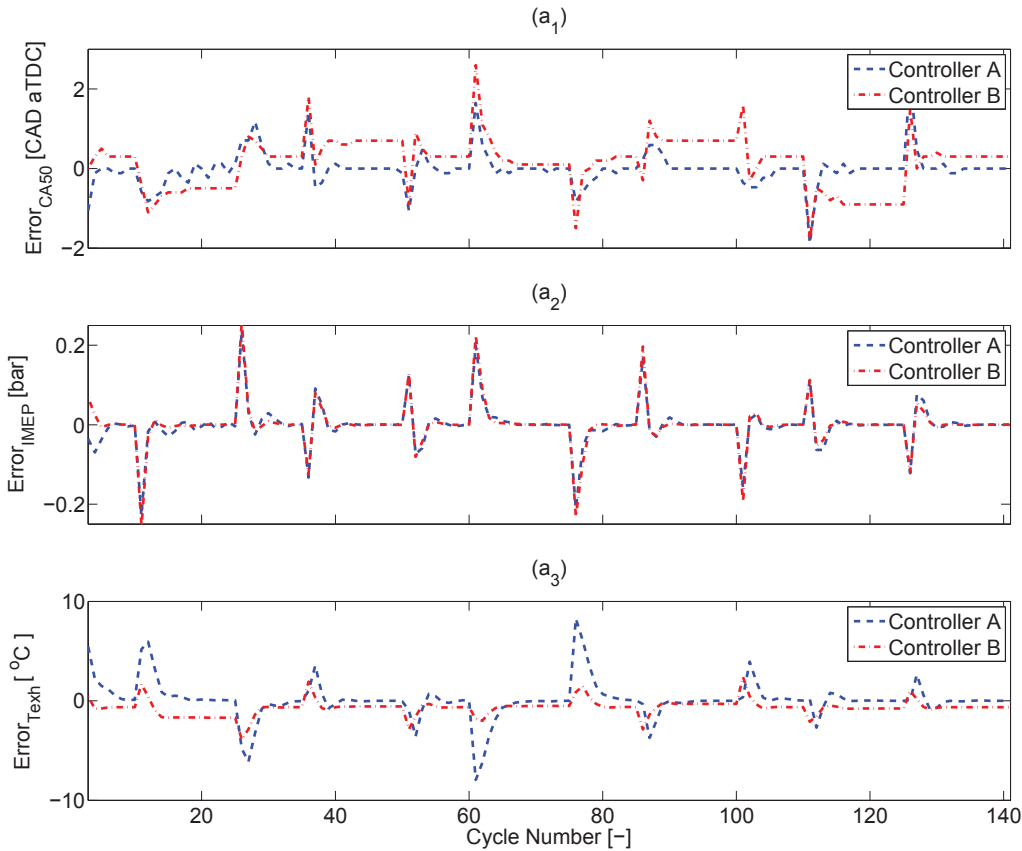


Figure 4.21: Tracking Error Comparison for Three-Input Three-Output, Type A (Fig.4.16) and Type B (Fig.4.17) Controllers for the Simultaneous Tracking Changes, where (a_x) are the Plant Outputs

Table 4.5
Tracking and Disturbance Rejection Performance of Three-Input Three-Output Controllers

Performance parameters	Controller A - Fig.4.16			Controller B - Fig.4.17		
	CA50	T_{exh}	IMEP	CA50	T_{exh}	IMEP
Rise time	2 cycles	2 cycles	1 cycle	1 cycle	1 cycle	1 cycle
Steady-state error	0 CAD	0°C	0 bar	0.1 CAD	0.1°C	0 bar
Maximum overshoot	0 CAD	0°C	0.02 bar	0 CAD	0.9°C	0.02 bar
Settling time	6 cycles	3 cycles	6 cycles	3 cycles	2 cycles	6 cycles
Dist. max. absolute deviation	1.2 CAD	8°C	0.09 bar	2.5 CAD	3.9°C	0.09 bar
Max. steady-state deviation	0 CAD	0.3°C	0 bar	0.9 CAD	1.7°C	0 bar
Dist. rejection speed	9 cycles	4 cycles	6 cycles	4 cycles	3 cycles	6 cycles

Chapter 5

Conclusion and Future Work

This thesis provided two major contributions including: (1) development of a novel three-input three-output controller to adjust major HCCI engine variables; and (2) establishment of an experimental HCCI engine setup with the main focus on developing prototype engine controllers and engine instrumentation. The following are some of the major outcomes from this thesis.

5.1 Summary

- An HCCI engine setup based on a 2-liter GM Ecotec LHU engine was developed. A total of twenty seven new sensors were installed on the engine. The new sensors include thermocouples, pressure transducers, in-cylinder pressure sensors, encoder, and lambda sensors. In addition three new actuators were installed on the engine to add further controllability to the engine. Actuators include ETC valve, EGR valve, and PFI injectors. The actuators were successfully tested using dSPACE controller units. The crank/cam synchronization to determine the firing TDC of the engine was

successfully performed and validated using in-cylinder pressure sensors.

- A COM was developed for an HCCI Ricardo engine for calculating CA50, T_{exh} , and IMEP. The COM was validated with actual experimental data for both steady state and transient engine conditions. The COM can predict CA50, T_{exh} , and IMEP for both steady state and transient engine operating conditions with average predicted error less than 1.8 CAD, 13.3 °C, and 0.3.
- A step by step progression was developed from SISO controllers to three-input three-output controllers for controlling CA50, T_{exh} , and IMEP using inputs including ON, P_{man} , and \dot{m}_{fuel} respectively. Empirical (PID and PI), and model-based (DSSMC) controllers were developed for controlling output parameters of a physical HCCI engine model. The simulation results showed that DSSMC controllers are faster in responding to step changes and have better disturbance rejection capability as compared to empirical PID controllers. Because of the mismatch between the COM and the physical HCCI model, the DSSMC controllers are found to have higher steady-state tracking errors.

5.2 Suggestions for Future Work

- From the engine experimental point of view there are several tasks which need to be carried out in order to complete a fully capable HCCI engine test setup. Some of the major tasks are increasing the engine compression ratio, adding port fuel injectors, adding a supercharger to the intake air path, controlling intake and exhaust cam phasers, controlling DI injectors' timing, and calibrating the engine to run in the HCCI mode.
- Future improvements in the COM can be done by removing simplifying modeling assumptions, thus the COM will become closer to the physical plant model. For

instance, the empirical relation for CA50 prediction can be improved by including the impacts of other engine parameters like N and T_{man} . This can help improve the accuracy of the designed model-based (DSSMC) controllers.

- A more accurate exhaust gas temperature model can be developed by adding gas flow dynamics. This will enhance the accuracy of the HCCI simulation test bed for evaluating T_{exh} controllers.
- For the state space model used to design the DSSMC, the disturbance matrix can be improved by incorporating a more detailed physical model in the COM. Thus, the model systematically shows the effects of disturbances like engine speed, intake manifold temperature, and EGR on combustion phasing and exhaust gas temperature. This will make the controller more robust against external disturbances.
- The controller developed in this thesis were decentralized. A potential area of improvement is to design centralized HCCI controller to minimize the disturbances caused by the control actions of other sub-controllers. Two examples of centralized engine controller are found in [60], [61].

References

- [1] *Energy Information Administration (EIA), US Department of Energy: Washington, DC [online]. Available: www.eia.doe.gov/emeu/aer, 2011.*

- [2] *California Air Resources Board (CARB) Emission Norms [Online]. Available:<http://www.dieselnet.com/standards/us/ld-ca.php>, 2014.*

- [3] *Total world energy. The World Bank Total Energy Usage [Online]. Available:<http://data.worldbank.org/indicator>. 2014.*

- [4] *World CO2 emission. The World Bank Total Carbon Dioxide Emissions [Online]. Available:<http://data.worldbank.org/indicator>, 2014.*

- [5] *Chu, S. The science of photons to fuel. Physics of Sustainable Energy: Using Energy Efficiently and Producing It Renewably, AIP Publishing, 1044(1),266-282, 2008.*

- [6] *Zhao, H. Homogeneous Charge Compression Ignition (HCCI) and Controlled Auto Ignition (CAI) Engines for the Automotive Industry, Woodhead, Brunel University, UK 2007.*

- [7] *Hultqvist, A.; Engdar, U.; Johansson, B.; Klingmann, J. Reacting Boundary Layers in Homogeneous Charge Compression Ignition (HCCI) Engine. SAE Technical Paper, 2001-01-1032, 2001.*

- [8] Hultqvist, A.; Christensen, M.; Johansson, B.; Richter, M.; Nygren, J.; Hult, J.; Aldén, M. *The HCCI Combustion Process in a Single Cycle-High-Speed Fuel Tracer LIF and Chemiluminescence Imaging*. SAE Technical Paper, 2002-01-0424, **2002**.
- [9] Saxena, S.; Bedoya, I. D. *Fundamental Phenomena Affecting Low Temperature Combustion and HCCI Engines, High Load Limits and Strategies for Extending these Limits*. *Progress in Energy and Combustion Science*, 39(5),457-488, **2013**.
- [10] Erlandsson, O. *Early Swedish Hot-Bulb Engines-Efficiency and Performance Compared to Contemporary Gasoline and Diesel Engines*. SAE Technical Paper, 2002-01-0115. **2002**.
- [11] Gussak, L.; Karpov, V.; Tikhonov, Y. V. *The Application of Lag-Process in Prechamber Engines*. SAE Technical Paper, 790692, **1979**.
- [12] Onishi, S.; Jo, S. H. *Active Thermo-Atmosphere Combustion (ATAC)—A New Combustion Process for Internal Combustion Engines*. SAE Technical Paper, 790501, **1979**.
- [13] Noguchi, M.; Tanaka, Y.; Tanaka, T.; Takeuchi, Y. *A study on Gasoline Engine Combustion by Observation of Intermediate Reactive Products During Combustion*. SAE Technical Paper, 790840, **1979**.
- [14] Najt, P. M.; Foster, D. E. *Compression-Ignited Homogeneous Charge Combustion*. SAE Technical Paper, 830264, **1983**.
- [15] Thring, R. *Homogeneous Charge Compression Ignition (HCCI) Engines*. SAE Technical Paper, 892068, **1989**.
- [16] Stockinger, V.; Schapertons, H.; Kuhlmann, U. *Investigations on a Gasoline Engine Working with Self-ignition by Compression*. *MTZ*, 53, 80-85, **1992**.
- [17] Olsson, J.-O.; Tunestål, P.; Johansson, B. *Closed-Loop Control of an HCCI Engine*. SAE Technical Paper, 2001-01-1031, **2001**.

- [18] Law, D.; Kemp, D.; Allen, J.; Kirkpatrick, G.; Copland, T. *Controlled Combustion in an IC-Engine with a Fully Variable Valve Train*. SAE Technical Paper, 2001-01-0251, **2001**.
- [19] Fuerhapter, A.; Piock, W. F.; Fraidl, G. *CSI: Controlled Auto Ignition: The Best Solution for The Fuel Consumption: Versus Emission Trade-Off?*. SAE Technical Paper, 2003-01-0754, **2003**.
- [20] Abuelsamid, S. *ABG Tech Analysis and Driving Impression: GM's HCCI Engine* [Online]. Available:<http://abg-tech-analysis-and-driving-impression-gms-hcci-engine/>, **2007**.
- [21] Nüesch, S.; Hellström, E.; Jiang, L.; Stefanopoulou, A. G. *Mode Switches among SI, SACI, and HCCI Combustion and their Influence on Drive Cycle Fuel Economy*, **2014**.
- [22] Christensen, M.; Hultqvist, A.; Johansson, B. *Demonstrating The Multi Fuel Capability of a Homogeneous Charge Compression Ignition Engine with Variable Compression Ratio*. SAE Technical Paper, 1999-01-3679, **1999**.
- [23] Johansson, T.; Johansson, B.; Tunestål, P.; Aulin, H. *HCCI Operating Range in a Turbo-Charged Multi Cylinder Engine with VVT and Spray-Guided DI*. SAE Technical Paper, 2009-01-0494, **2009**.
- [24] Ravi, N. *Modeling and Control of Exhaust Recompression HCCI Using Variable Valve Actuation and Fuel Injection*, PhD thesis, Stanford University, **2010**.
- [25] Anderson Jr, J. D. *Fundamentals of Aerodynamics*. Tata McGraw-Hill Education, New York, **1985**.
- [26] DOE. *Homogeneous Charge Compression Ignition (HCCI) Technology, A Report to the US Congress*. US Department of Energy, Energy Efficiency and Renewable Energy, Office of Transportation Technologies, **2001**.

- [27] Stanglmaier, R. H.; Roberts, C. E. *Homogeneous Charge Compression Ignition (HCCI): Benefits, Compromises, and Future Engine Applications*. SAE Technical Paper, 1999-01-3682, **1999**.
- [28] Shahbakhti, M.; Ghazimirsaied, A.; Koch, C. *Experimental Study of Exhaust Temperature Variation in a Homogeneous Charge Compression Ignition Engine*. *Proceedings of the Institution of Mechanical Engineers, Part D: Journal of Automobile Engineering*, 224(9), 1177-1197, **2010**.
- [29] Dehghani Firoozabadi, M.; Shahbakhti, M.; Koch, C.; Jazayeri, S. *Thermodynamic Control-Oriented Modeling of Cycle-to-Cycle Exhaust Gas Temperature in an HCCI Engine*. *Applied Energy*, 110, 236-243, **2013**.
- [30] Lu, X.-c.; Chen, W.; Hou, Y.-c.; Huang, Z. *Study on The Ignition, Combustion and Emissions of HCCI Combustion Engines Fueled with Primary Reference Fuels*. SAE Technical Paper, 2005-01-0155, **2005**.
- [31] Ferrari, V.; Honorato, R. L. *Achieving EURO III and EURO IV with Ultra-Low Precious Metal Loadings*. SAE Technical paper, 2007-01-2565, **2007**.
- [32] Tanikawa, K.; Hirota, T.; Yamada, T.; Komori, M.; Zhang, G.; Muraki, H. *Development of Advanced Three-Way Catalyst Technology*. SAE Technical paper, 2008-01-1645, **2008**.
- [33] Caraceni, A.; Cioffi, V.; Garofalo, F.; Senatore, A.; Vittorioso, G.; Barberio, C. *Emission Control Technologies for EU Stage IV+ EOBD on Small Cars (Part I): Pre-Screening of Potential Solutions*. SAE Technical paper, 1999-01-0775, **1999**.
- [34] Pipitone, E.; Beccari, A. *Determination of TDC in Internal Combustion Engines by A Newly Developed Thermodynamic Approach*. *Applied Thermal Engineering*, 30(14), 1914-1926, **2010**.

- [35] Bidarvatan, M.; Shahbakhti, M.; Jazayeri, S. A. *Model-Based Control of Combustion Phasing in an HCCI Engine*. SAE Technical paper, 2012-01-1137, **2012**.
- [36] Bidarvatan, M.; Shahbakhti, M. *Two-Input Two-Output Control of Blended Fuel HCCI Engines*. SAE Technical paper, 2013-01-1663, **2013**.
- [37] Shahbakhti, M.; Koch, C. *Characterizing The Cyclic Variability of Ignition Timing in an HCCI Engine Fueled with n-Heptane/iso-Octane Blend Fuels*. *International Journal of Engine Research*, 9(9), 361-397, **2008**.
- [38] Heywood, J. B. *Internal Combustion Engine Fundamentals*. McGraw-hill New York **1988**.
- [39] Swan, K.; Shahbakhti, M.; Koch, C. R. *Predicting Start of Combustion Using A Modified Knock Integral Method for an HCCI Engine*. SAE Technical Paper, 2006-01-1086, **2006**.
- [40] Shahbakhti, M.; Lupul, R.; Koch, C. R. *Sensitivity Analysis & Modeling of HCCI Auto-Ignition Timing*. *Advances in Automotive Control*, 5(1), 303-310, **2007**.
- [41] Gorzelic, P.; Hellström, E.; Stefanopoulou, A.; Li, J. *Model-Based Feedback Control for an Automated Transfer Out of SI Operation During SI to HCCI Transitions in Gasoline Engines*. ASME 2012 5th Annual Dynamic Systems and Control Conference, **2012**.
- [42] Shahbakhti, M.; Koch, C. R. *Physics Based Control Oriented Model for HCCI Combustion Timing*. *Journal of Dynamic Systems, Measurement, and Control*, 132(2), **2010**.
- [43] Ravi, N.; Roelle, M. J.; Liao, H.-H.; Jungkunz, A. F.; Chang, C.-F.; Park, S.; Gerdes, J. C. *Model-Based Control of HCCI Engines Using Exhaust Recompression*. *Control Systems Technology, IEEE*, 18(6), 1289-1302, **2010**.

- [44] Shaver, G. M.; Gerdes, J. C.; Roelle, M. J. *Physics-Based Modeling and Control of Residual-Affected HCCI Engines. Journal of Dynamic Systems, Measurement, and Control*, 131(2), **2009**.
- [45] Bengtsson, J.; Strandh, P.; Johansson, R.; Tunestål, P.; Johansson, B. *Hybrid Modelling of Homogeneous Charge Compression Ignition (HCCI) Engine Dynamics - A Survey. International Journal of Control, Taylor & Francis*, 80(11), 1814-1847, **2007**.
- [46] Widd, A.; Liao, H.-H.; Gerdes, J. C.; Tunestål, P.; Johansson, R. *Hybrid Model Predictive Control of Exhaust Recompression HCCI. Asian Journal of Control*, 16(2), 370-381, **2014**.
- [47] Bidarvatan, M.; Shahbakhti, M.; Jazayeri, S.; Koch, C. *Cycle-to-Cycle Modeling and Sliding Mode Control of Blended-Fuel HCCI Engine. Control Engineering Practice*, 24, 79-91, **2014**.
- [48] Ebrahimi, K.; Koch, C. R. *HCCI Combustion Timing Control with Variable Valve Timing. American Control Conference*, **2013**.
- [49] Chiang, C.-J.; Huang, C.-C.; Jankovic, M. *Discrete-Time Cross-Term Forwarding Design of Robust Controllers for HCCI Engines. American Control Conference*, **2010**.
- [50] Schauer, F. X.; Zimmer, T.; Bachhuber, M.; Scheller, M.; Yamasaki, Y.; Oryoji, K.; Wachtmeister, G. *Development of a Model-Based HCCI Control Strategy for an Engine with a Fully Variable Valve Train. SAE Technical Paper, 2013-01-1667*, **2013**.
- [51] Erlien, S. M.; Jungkunz, A. F.; Gerdes, J. C. *Multicylinder HCCI Control With Coupled Valve Actuation Using Model Predictive Control. Journal of Dynamic Systems, Measurement, and Control*, 135 **2013**.

- [52] Shaver, G. M.; Gerdes, J. C.; Roelle, M. *Physics-Based Closed-Loop Control of Phasing, Peak Pressure and Work Output in HCCI Engines Utilizing Variable Valve Actuation. American Control Conference, 2004.*
- [53] Bidarvatan, M.; Shahbakhti, M. *Integrated HCCI Engine Control Based on a Performance Index. Journal of Engineering for Gas Turbines and Power, 136(10), 2014.*
- [54] Maurya, R. K.; Agarwal, A. K. *Experimental Investigation of Close-Loop Control of HCCI Engine Using Dual Fuel Approach. SAE Technical Paper, 2013-01-1675, 2013.*
- [55] Hellstrom, E.; Larimore, J.; Jade, S.; Stefanopoulou, A. G.; Jiang, L. *Reducing Cyclic Variability While Regulating Combustion Phasing in a Four-Cylinder HCCI Engine. Control Systems Technology, IEEE, 3(22), 1190-1197,.*
- [56] Ziegler, J.; Nichols, N. *Optimum Settings for Automatic Controllers. Journal of Dynamic Systems, Measurement, and Control, 115(2B), 220-222, 1993.*
- [57] Franklin, G. F.; Workman, M. L.; Powell, D. *Digital Control of Dynamic Systems. Addison-Wesley Longman Publishing, 1997.*
- [58] Yu, W.-C.; Wang, G.-J. *Discrete Sliding Mode Controller Design Based on The LQR Suboptimal Approach with Application on AC servo Motor. Journal of the Chinese Institute of Engineers, Taylor & Francis, 29(5), 873-882, 2006.*
- [59] Milosavljevic, C. *General Conditions for The Existence of a Quasi-Sliding Mode on The Switching Hyperplane in Discrete Variable Structure Systems. Automation and Remote Control, New York, 46(3), 307-314, 1985.*
- [60] Zentner, S.; Asprion, J.; Onder, C.; Guzzella, L. *An equivalent emission minimization strategy for causal optimal control of diesel engines. Multidisciplinary Digital Publishing Institute, 7(3), 1230-1250, 2014.*

- [61] Shahbakhti, M.; Amini, M. R.; Li, J.; Asami, S.; Hedrick, J. K. *Early Model-Based Design and Verification of Automotive Control System Software Implementations. ASME Journal of Dynamic Systems, Measurement and Control* **2014**.
- [62] dSPACE. *Technical Manual of dSPACE RapidPro and MicroAutoBox*, **2013**.

Appendix A

Acronyms for different LTC Engines

There are many names given by different researchers to nearly the same field of study for LTC engines. Table A.1 summarizes some common names with their acronym forms. All these LTC engines are having two things common at minimal; (1) premixing of Air fuel mixture, and (2) Auto ignition combustion, which are the prime factors for HCCI combustion.

Table A.1
Acronym of Different LTC Engines

Acronym	Meaning	Researchers and Reference Year	Location
ATAC	Active thermo-atmosphere combustion	Onishi, 1979	Nippon Clean Engine Research Institute
TS	Toyota-Soken combustion	Noguchi, 1979	Toyota/Soken
CIHC	Compression-ignited homogeneous charge	Najt, 1983	University of Wisconsin-Madison
HCCI	Homogeneous charge compression ignition	Thring, 1989	SwRI
HiMICS	Homogeneous charge intelligent multiple injection combustion system	Yokota, 1997	Hino
MULDIC	Multiple stage diesel combustion	Hashizume, 1998	New ACE
MK, M-fire	Modulated kinetics	Kimura, 1999	Nissan
PCI	Premixed compression ignited combustion	Iwabuchi, 1999	Mitsubishi
PREDIC	Premixed diesel combustion	Yoshiaki, 2001	New ACE
UNIBUS	Uniform bulky combustion system	Yanagihara, 2001	Toyota
NADI	Narrow Angle Direct Injection	Gatellier, 2002	Institut Français Du Pétrole (IFP)
AR, ARC	Active radical combustion	Ishibashi, 2004	Honda
RCCI	Reactivity charged controlled ignition	Reitz, 2010	University of Wisconsin, Madison

Appendix B

MSc. Publication

1. D. Kothari, M. Bidarvatan, M. Shahbakhti, "Modeling and Integrated Control of Exhaust Gas Temperature, Load, and Combustion Phasing in an HCCI Engine", Under preparation for submission to *IEEE Transactions on Vehicular Technology*.

Appendix C

Thesis Files Summary

Following are the list of tables referring experimental data files, matlab/simulink files (model, code and figure) and visio diagrams and figures for studying and developing results for this thesis.

1. Table C.1: .MAT files (Experimental data)
2. Table C.2: .Slx files (Simulink models)
3. Table C.3: Documents
4. Table C.4: .m files (Matlab codes)
5. Table C.5: .fig files (Matlab plots)
6. Table C.6: Visio files (Thesis Images)

Table C.1
Experimental Data Files (.mat files)

Sr #	File name	Description
1	ExpData_Oct26_Test5	Experimental data points for validating COM
2	ExhValveProfileLift	Exhaust valve profile lift [mm]
3	ExhValveProfileCrankAngle	Exhaust valve profile with respect to crank angle
4	volume	In-cylinder volume for one complete cycle
5	RoverHead_Oct23_09	Experimental data for steady state validation

Table C.2
Simulink Models Files (.slx files)

Sr #	File name	Description
1	Controller_A	PID and PI controller model
2	Controller_B	DSSMC and PI controller model
3	Linearizing_COM	Linearizing nonlinear COM
4	Thermocouple_Lag	Thermocouple compensation
5	Egr_valve_controller	dSPACE EGR valve controller model
6	ETC_valve_model	dSPACE ETC valve controller model
7	Lambda_sensor	dSPACE lambda sensor model
8	MAP_sensor	dSPACE MAP sensor model
9	THMM_Thermoscan_CAN_model	dSPACE THMM CAN model
10	Overall_Engine_Simulink	dSPACE engine control model

Table C.3
Documents

Sr #	File name	Description
1	Thesis_Latex_zip	Thesis in latex code
2	dSPACE.doc	Self made dSPACE document
3	Defense_ppt	Defense presentation

Table C.4
Matlab Script Files (.m files)

Sr #	File name	Description
1	Detailed_Physical_Plant_model	HCCI plant model
2	MKIM_model	MKIM model
3	Control_oriented_model	COM model
4	CA50_parameterizing_1	For CA50 parameterization
5	CA50_parameterizing_2	For CA50 parameterization
6	state_space_nonlennear_model	Nonlinear COM
7	observer_CA50	CA50 observer
8	observer_Texh	T_{exh} observer
9	DSSMC_CA50	CA50 DSSMC
10	DSSMC_Texh	T_{exh} DSSMC
11	Data_points_MKIM	For MKIM operating points
12	Control_oriented_model_plot	For COM transient validation
13	Comparision_Plot_ControllerA_ControllerB	Comparing controllers
14	Crank_and_incyylinder_pressure_signal_relation	Crank synchronization
15	ETC_EGR_controller_performances	ETC and EGR control data

Table C.5
Matlab Figures Files (.fig files)

Sr #	File name	Description
1	ETC_controller	Fig.2.8
2	EGR_controller	Fig.2.10
3	Incylinder_pressure_and_crank_angle	Fig.2.11
4	PFI_and_crankangle	Fig.2.12
5	CA50_correlation	Fig.3.1
6	CA50_SS_validation	Fig.3.2
7	Texh_SS_validation	Fig.3.4
8	IMEP_SS_validation	Fig.3.5
9	COMvalidation	Fig.3.6
10	CA50_PID	Fig.4.3
11	CA50_DSSMC	Fig.4.5
12	Texh_PID	Fig.4.7
13	Texh_DSSMC	Fig.4.9
14	CA50_Texh_PID_single_tracking	Fig.4.11
15	CA50_Texh_PID_simultaneous_tracking	Fig.4.12
16	CA50_Texh_DSSMC_single_tracking	Fig.4.14
17	CA50_Texh_DSSMC_simultaneous_tracking	Fig.4.15
18	3_in_3_out_PID_DSSMC_single_comparision	Fig.4.18
19	3_in_3_out_PID_DSSMC_simulteneous_comparision	Fig.4.19
20	Error_3_in_3_out_plot_single_tracking	Fig.4.20
21	Error_3_in_3_out_plot_simulatenous_tracking	Fig.4.21

Table C.6
Vision Drawings/Images Files

Sr #	File name	Description
1	USA_Energy_distribustion	Fig.1.1
2	HCCI_adv_and_dis_adv	Fig.1.2
3	SI_vs_CI_vs_HCCI	Fig.1.3
4	HCCI_Cycle	Fig.1.4
5	Thesis_Organizaion	Fig.1.5
6	Engine_Geomrty_Catia	Fig.2.1
7	Engine_Valve_Timing	Fig.2.2
8	Engine_Experimental_Setup	Fig.2.3
9	Actual_Engine_Setup	Fig.2.4
10	Control_Structure	Fig.2.5
11	Simulink_blockset	Fig.2.6
12	Lambda_Sensor_Screen_Short	Fig.2.7
13	Lambda_sensor_position	Fig.2.4.1
14	EGRvalve_bothside	Fig.2.9
15	Crank_Cam_screenshot	Fig.2.4.4
16	Sensor_and_controller	Fig.2.13
17	Actuator_and_Controller	Fig.2.14
18	Exhaust_Pipe_Diagram	Fig.3.3
19	Control_Background	Fig.4.1
20	CA50_PID_controller	Fig.4.2
21	Texh_PID_controller	Fig.4.4
22	CA50_DSSMC	Fig.4.6
23	Texh_DSSMC	Fig.4.8
24	CA50_Texh_PID_controller	Fig.4.10
25	CA50_Texh_DSSMC	Fig.4.13
26	Controller_A	Fig.4.16
27	Controller_B	Fig.4.17